

## Voltage-induced modulation of the magnetic exchange in binuclear Fe(III) complex deposited on Au(111) surface

Nicolás Montenegro-Pohlhammer<sup>a,b\*</sup>, Gloria Cárdenas-Jirón<sup>c</sup>, Carmen J. Calzado<sup>d</sup>

<sup>a</sup>*Escuela de Ingeniería Civil, Facultad de Ingeniería, Ciencia y Tecnología, Universidad Bernardo O'Higgins, Santiago, Chile.*

<sup>b</sup>*Universidad Bernardo O'Higgins, Centro Integrativo de Biología y Química Aplicada (CIBQA), General Gana 1702, Santiago, Chile*

<sup>c</sup>*Laboratory of Theoretical Chemistry, Faculty of Chemistry and Biology, University of Santiago de Chile (USACH), Santiago, Chile.*

<sup>d</sup>*Departamento de Química Física. Universidad de Sevilla, c/ Prof. García González, s/n 41012. Sevilla, Spain.*

### Supporting Information

#### Contents

<b>S1. Magnetic properties of complex 1 in the gas phase</b> .....	<b>3</b>
S1.1. CASSCF active space orbitals .....	3
S1.2. Density Functional Theory (DFT) calculations.....	3
S1.2.1 Broken Symmetry (BS) theoretical background .....	3
S1.2.2 PBE + U studies.....	4
<b>S2. Deposition of complex 1 over the Au(111) surface</b> .....	<b>7</b>
S2.1. Computational details .....	7
<b>S3. Effects of the applied bias voltage on the magnetic coupling</b> .....	<b>9</b>
S3.1 Description of the employed surface-complex-STM molecular junction setup .....	9
S3.2 Complex 1 frontier orbitals diagrams in the three employed architectures .....	11
S3.3 Hay, Thibault and Hoffmann (HTH) model.....	12
S3.4 Effects of a homogeneous electric field in the complex in gas phase .....	17
S3.5 Potential iso-isolines and voltage-induced charge density in the junction setup .....	18
S3.5.1 Orientation 4 .....	18
S3.5.2 Orientation 1 .....	19
<b>S4. Frontier orbitals of the isolated complex</b> .....	<b>20</b>
S4.1. High Spin (HS) spin up frontier orbitals .....	20
S4.2. High Spin (HS) spin down frontier orbitals .....	21
S4.3. Broken Symmetry (BS) spin up frontier orbitals .....	22

S4.3. Broken Symmetry (BS) spin down frontier orbitals .....	23
<b>S5. Molecular projected self-consistent Hamiltonian (MPSH) states of the complex .....</b>	<b>24</b>
S5.1. Orientation 1 .....	24
S5.1.1 High Spin (HS) spin up frontier orbitals .....	24
S5.1.2 High Spin (HS) spin down frontier orbitals.....	25
S5.1.3 Broken Symmetry (BS) spin up frontier orbitals .....	26
S5.1.4 Broken Symmetry (BS) spin down frontier orbitals.....	27
S5.2. Orientation 4 .....	28
S5.2.1 High Spin (HS) spin up frontier orbitals .....	28
S5.2.2 High Spin (HS) spin down frontier orbitals.....	29
S5.2.3 Broken Symmetry (BS) spin up frontier orbitals .....	30
S5.2.4 Broken Symmetry (BS) spin down frontier orbitals.....	31
<b>References.....</b>	<b>32</b>

## S1. Magnetic properties of complex 1 in the gas phase

### S1.1. CASSCF active space orbitals

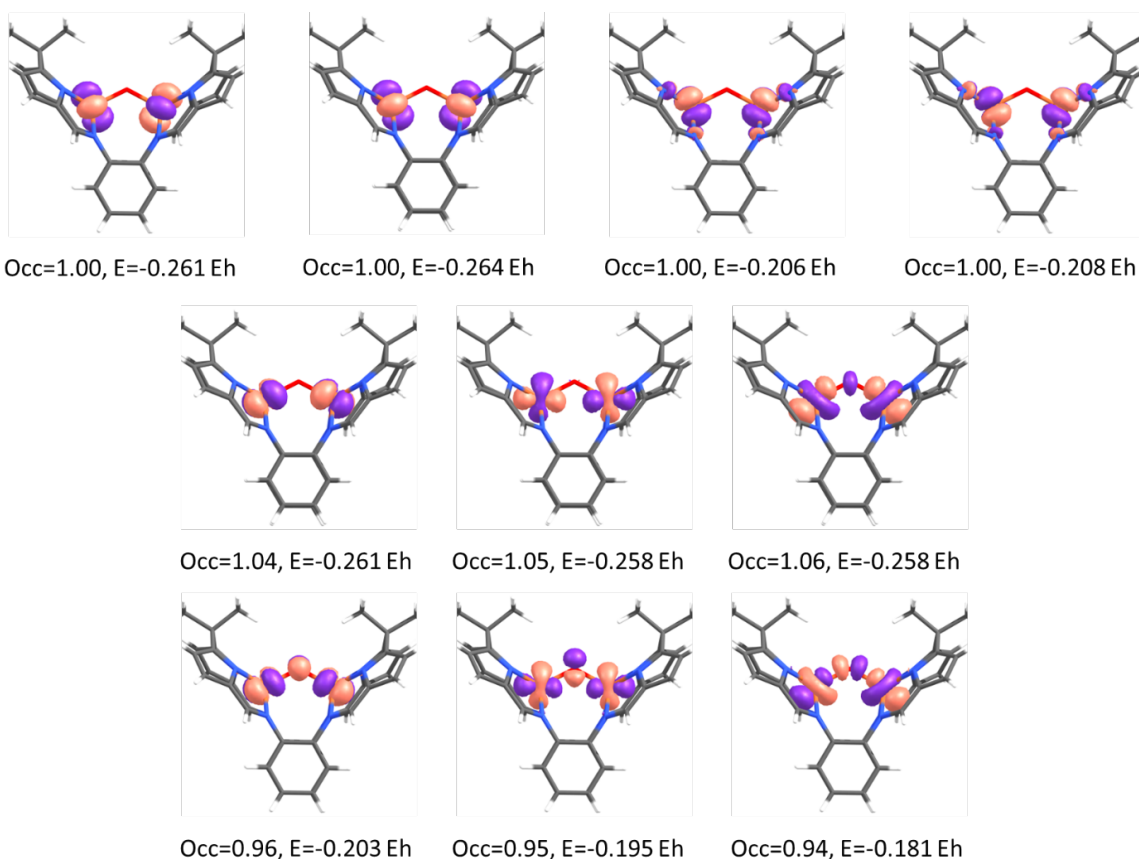


**Figure S1.1.** Active orbitals employed for the CASSCF calculation performed in this work.

### S1.2. Density Functional Theory (DFT) calculations

#### S1.2.1 Broken Symmetry (BS) theoretical background

The Spin Hamiltonian (SH) is a particular case of effective Hamiltonian, used to study the interaction between any kind of spin carrier. In this model all orbital coordinates are removed and replaced by only spin coordinates. For two magnetic centers in the absence of an external magnetic field it can be written as:

$$\hat{H} = -J\hat{S}_1 \cdot \hat{S}_2 + D \sum_{i=1,2} \left[ \hat{S}_{i,z}^2 - \frac{1}{3}S(S+1) \right] + R \sum_{i=1,2} [\hat{S}_{i,x}^2 - \hat{S}_{i,y}^2]$$

where  $\hat{S}_i$  are the local spin operators, J is the isotropic coupling constant, D and R are the single-ion axial and rhombic zero field splitting parameters respectively, and S is the global spin of the system. In most

cases the first term is dominant, and the remaining are included as perturbations, in this case the last equation is reduced to:

$$\hat{H} = -J\hat{S}_1 \cdot \hat{S}_2$$

also known as the “Heisenberg–Dirac–Van-Vleck Spin-Hamiltonian” (HDVV). The energy of each state with total spin S is given by:<sup>1</sup>

$$E(S) = \frac{J}{2}[S(S + 1) - S_1(S_1 + 1) - S_2(S_2 + 1)]$$

where the energy between adjacent spin levels can be expressed as:

$$E(S - 1) - E(S) = JS$$

and J can be computed as:

$$J = \frac{E(S - 1) - E(S)}{S}$$

By means of the DFT, the isotropic coupling constant J was calculated for **1** using the Broken Symmetry (BS) method introduced by Noodleman<sup>2</sup>. The orbitals used for the High Spin (HS) state were obtained from SCF optimization of the S = 5, M<sub>s</sub> = 5 unrestricted determinant. The BS determinant is constructed taking the HS determinant as a reference and flipping the spin density localized on one of the Fe(III) ions, followed by the corresponding SCF energy optimization. The magnitude of the coupling constant J is then calculated in terms of the energy  $E_{HS,BS}$  and the spin expectations value  $\langle S^2 \rangle_{HS,BS}$  of this two determinants, using the expression proposed by Yamaguchi *et al.*<sup>3</sup> :

$$J = \frac{2(E_{BS} - E_{HS})}{\langle S^2 \rangle_{HS} - \langle S^2 \rangle_{BS}}$$

with  $\langle S^2 \rangle_{HS} = \left(\frac{1}{2} \cdot \mu_{\beta}^{HS}\right) \cdot \left(\frac{1}{2} \cdot \mu_{\beta}^{HS} + 1\right)$  and  $\langle S^2 \rangle_{BS} = \left(\frac{1}{2} \cdot \mu_{\beta}^{BS}\right) \cdot \left(\frac{1}{2} \cdot \mu_{\beta}^{BS} + 1\right)$ , where  $\mu_{\beta}^{HS}/\mu_{\beta}^{BS}$  is the effective magnetic moment of the complex in the High Spin (HS)/Broken Symmetry (BS) solutions.

### S1.2.2 PBE + U studies

Although the inherent multireference nature of the different spin states wave functions makes Wave Function-based (WFT) the natural and most accurate way to evaluate the magnetic properties, it has shown that the BS method, in combination with hybrid exchange-correlation (XC) functionals, to be a viable alternative to WFT at the time of computing J in several systems.<sup>4-6</sup> However, both WFT and DFT methods employing hybrid functionals are computationally costly, and their application further than

molecular systems and small extended systems is prohibitive, not to mention in DFT-NEGF calculations; thus, it is imperative to find DFT-based methods using the more affordable GGA XC functionals capable of balancing accuracy and computational cost to study the magnetic and transport properties in complex systems like the ones mentioned above.

In order to establish a methodology that balances computational cost with accuracy, we started by computing complex **1** magnetic coupling constant  $J$  through the BS methodology utilizing the PBE0 hybrid XC functional.<sup>7</sup> We used the obtained  $J$  value ( $-207.89 \text{ cm}^{-1}$ ) as a reference for our future tests, on the one hand, because there is no experimental data available, and on the other, based on recent study where it is shown that the PBE0 functional provides accurate  $J$  values in both dinuclear and poly nuclear  $\text{Fe}_2(\text{III})$  complexes.<sup>8</sup> In addition, the obtained  $J$  value is in line with experimentally reported ones (ranging from  $-160$  to  $-215 \text{ cm}^{-1}$ ) in similar  $\mu$ -oxo bridged  $\text{Fe}_2(\text{III})$  pentacoordinate complexes.<sup>9-12</sup>

Next, we performed a series of DFT calculations on the isolated complex, employing the computationally efficient Perdew–Burke–Ernzerhof (PBE)<sup>13</sup> exchange-correlation (XC) functional along with an on-site Hubbard  $U$  correction to the iron d-type orbitals,<sup>14-16</sup> with the aim of finding an appropriate value of  $U_{\text{eff}}$  capable of describing the magnetic properties of the complex but at low computational cost. This methodology, known as PBE+ $U$ , has been widely employed to study the magnetic properties of organometallic complexes deposited over different substrates,<sup>17-19</sup> as well as to probe their transport properties as molecular active elements in molecular junctions architectures through DFT+ $U$ -NEGF methods.<sup>20-23</sup> Our tests determined that a value of  $U_{\text{eff}} = 4.0 \text{ eV}$  not only accurately reproduced the  $J$  value computed with the hybrid PBE0 XC functional (Table S1) but also the frontier orbitals shape (Figure S4.2), as well as to drastically improved the HOMO-LUMO gap (with respect to the GGA PBE functional) (Figure S1.2), in both the high spin (HS) and the broken symmetry (BS) states. Moreover, it is worth remarking that they significantly differ from the MOs obtained employing the PBE functional without Hubbard correction, so caution is advised at the time of evaluating properties highly dependent on the shape of these orbitals like, for instance, the transport properties in molecular junctions. We adopted the PBE+ $U$  approach in all the following studies focused on the interaction of **1** with an Au(111) surface, an STM tip, and the effects that the voltage has on  $J$  employing a surface-complex-STM molecular junction like setup.

All the above calculations were performed by means of the Quantumwise ATK software package,<sup>24</sup> representing all atoms using a double- $\zeta$ -polarized (DZP) basis set, along with PseudoDojo norm-conserving pseudopotentials.<sup>25</sup> The mesh cut-off energy was set to 210 Rydberg for both the real and reciprocal space

grids in all calculations, with a self-consistency tolerance for the convergence of the Hamiltonian and density matrices of  $1.0 \times 10^{-4}$  eV.

**Table S1** Calculated values of  $J$  on complex 1 employing different XC functionals and methodologies.

Methodology	$J$ ( $\text{cm}^{-1}$ )
PBE	-405.97
PBE + U(4 eV)	-214.02
PBE0	-207.89

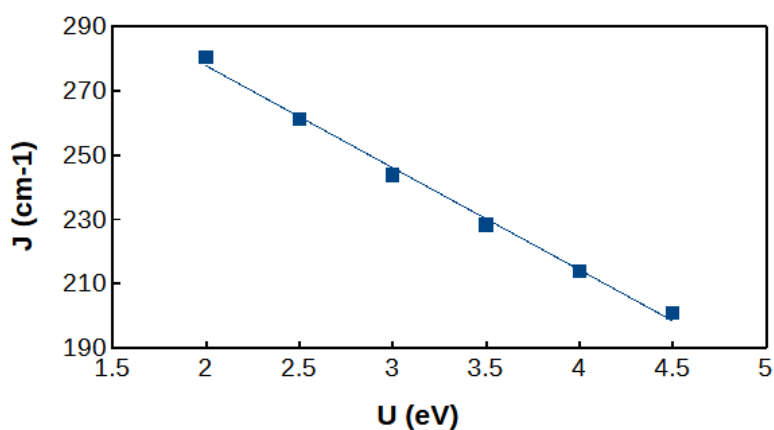


**Figure S1.2.** Coupling constant  $J$  dependence on the utilized  $U_{\text{eff}}$  parameter.

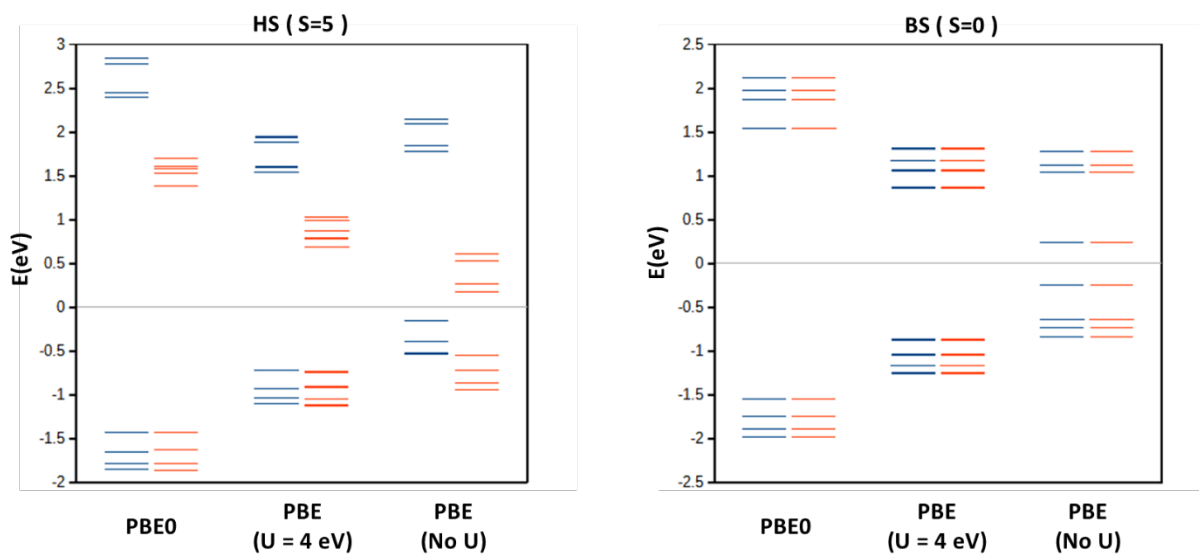


**Figure S1.3.** Frontier orbitals diagrams computed for complex **1** in the High Spin (HS) and Broken Symmetry (BS) solutions, employing the PBE0 hybrid XC functional, PBE GGA XC functional, and the PBE XC functional along with  $U_{\text{eff}} = 4.0$  eV.

## S2. Deposition of complex **1** over the Au(111) surface

### S2.1. Computational details

All the geometry optimizations required for the deposition of **1** over the Au(111) surface, as well as the NEGF-DFT studies conducted on the surface-complex-STM molecular junctions, were performed using the Quantumwise ATK software package employing the PBE+U methodology described in section S1.2 for the isolated complex. In addition, the Van der Waals interactions were considered through the DFT-D3 method of Grimme<sup>26</sup>.

We study the deposition of **1** over the Au(111) surface in four initial orientations (Figure S2.1), employing, in all cases, a gold slab of 3 layers of 8x8 Au atoms. All of the complex **1** atoms were allowed to relax in addition to the 64 gold atoms of the first layer of the surface, and fixing the positions of the atoms of the lower two layers (Figure S3.1.a). The coupling constant  $J$  was computed in the deposited systems through the BS methodology, as is described above for the isolated complex case.

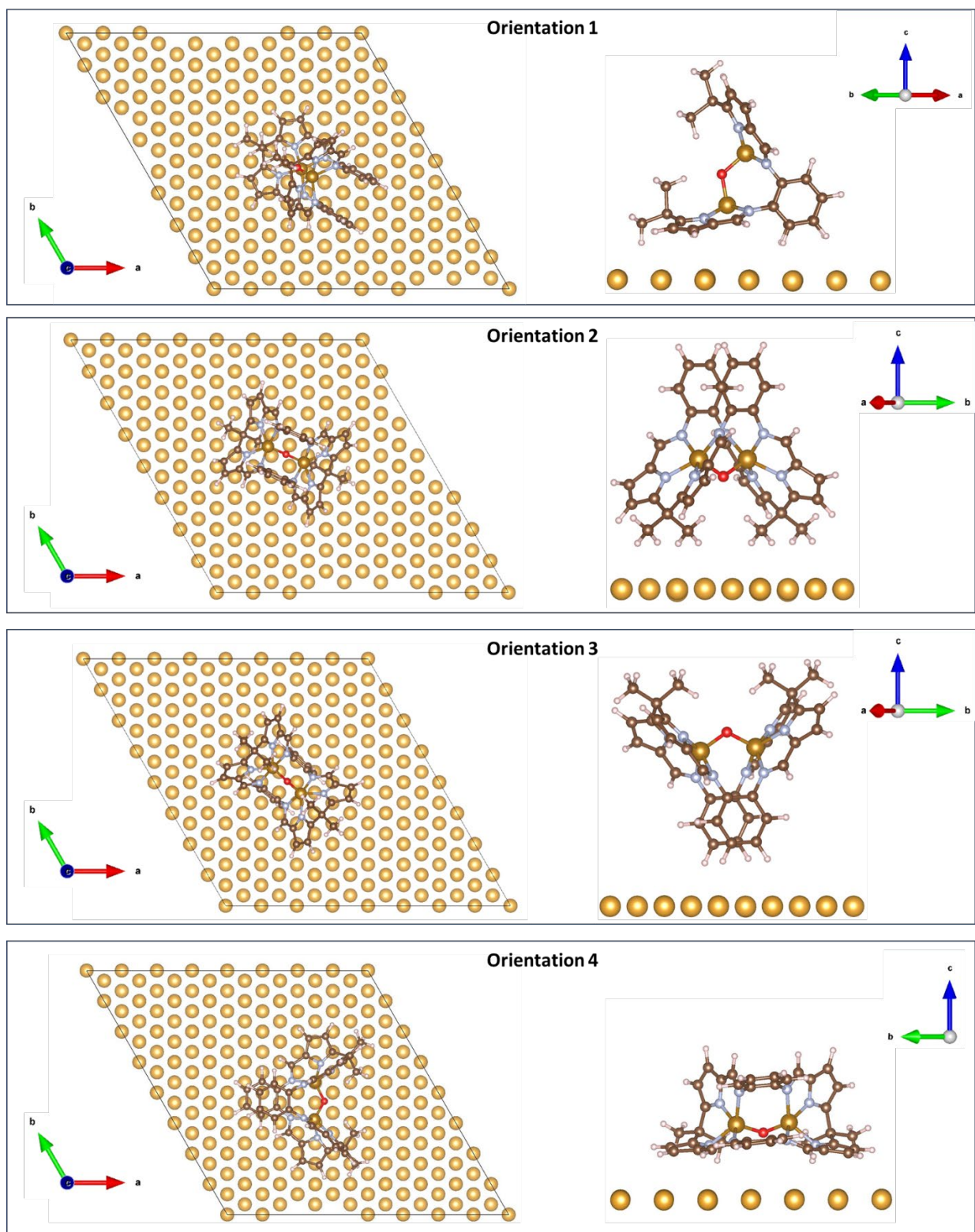


**Figure S2.1** Optimized geometry adopted by complex 1 after the deposition over the Au(111) surface in the four studied orientations.

Before studying the effects that the applied bias voltage would have on complex 1 magnetic properties in a surface-complex-STM-like setup, simulating an open system through the NEGF-DFT methodology, we probe the effects that a pyramidal-like Au cluster would have in the electronic structure of the molecule@Au(111)-slab system. Using the same unit cell, but increasing the C lattice vector length, we study the effects of an STM on the complex in orientations 1 and 4, adding a pyramidal 39 Au-atoms cluster at 3 Å from the higher H atoms of the molecule (Figure S3.1.b). The main reason behind this analysis is that, due to the size of the molecular junction setup, added to the high computational cost of the NEGF-DFT calculations (especially when a finite voltage is applied), we had to “cut” the size of the Au surface slab in the directions perpendicular to the transport direction (from 64 to 30 Au atoms), adding the corresponding empty space to avoid the interaction of the scattering zone periodic images; and we wanted to check the impact that this approximation would have in the electronic structure of the deposited complex. As shown in Figure S3.2 and in Section S5, both the frontier orbitals energies and wavefunctions are practically unaffected by adopting the approximation stated above, where the only observable difference is a slight stabilization of the frontier orbitals in the molecular junction setup at zero bias. In addition, it is also observed that the addition of the Au pyramidal cluster does not have a differential effect on the electronic structure of the deposited complex in the slab configuration, as well as in the magnitude of the computed J value (Table S2).

**Table S2.** Calculated values of J (cm<sup>-1</sup>) for complex 1 for each deposition orientation in the three configurations employed throughout this work.

	<b>Surface</b>	<b>Slab + pyramid cluster</b>	<b>Junction</b>
Orientation 1	204.60	204.50	204.54
Orientation 2	197.27	-	-
Orientation 3	200.02	-	-
Orientation 4	196.89	196.72	197.67

### S3. Effects of the applied bias voltage on the magnetic coupling

#### S3.1 Description of the employed surface-complex-STM molecular junction setup

To probe the effects an applied voltage bias would have on the deposited complex, we simulated a surface-molecule-STM molecular-junction-like setup (Figure S3.1.c), simulating an open system through the NEGF-DFT methodology.<sup>27</sup> For the scattering zone of the molecular junctions, we utilized a portion of the Au(111)

surface consisting of six layers of  $6 \times 5$  atoms as the left electrode extension and 8 interleaved layers of 12 and 13 gold atoms ending in a pyramid shape consisting of three layers of 9, 4, 1 atoms each, to simulate the STM tip, as the right electrode extension. A vacuum space of  $20 \text{ \AA}$  has been added in the transverse directions for both the electrodes and the scattering zone, in order to avoid interactions with the corresponding periodic repetitions in these axes.

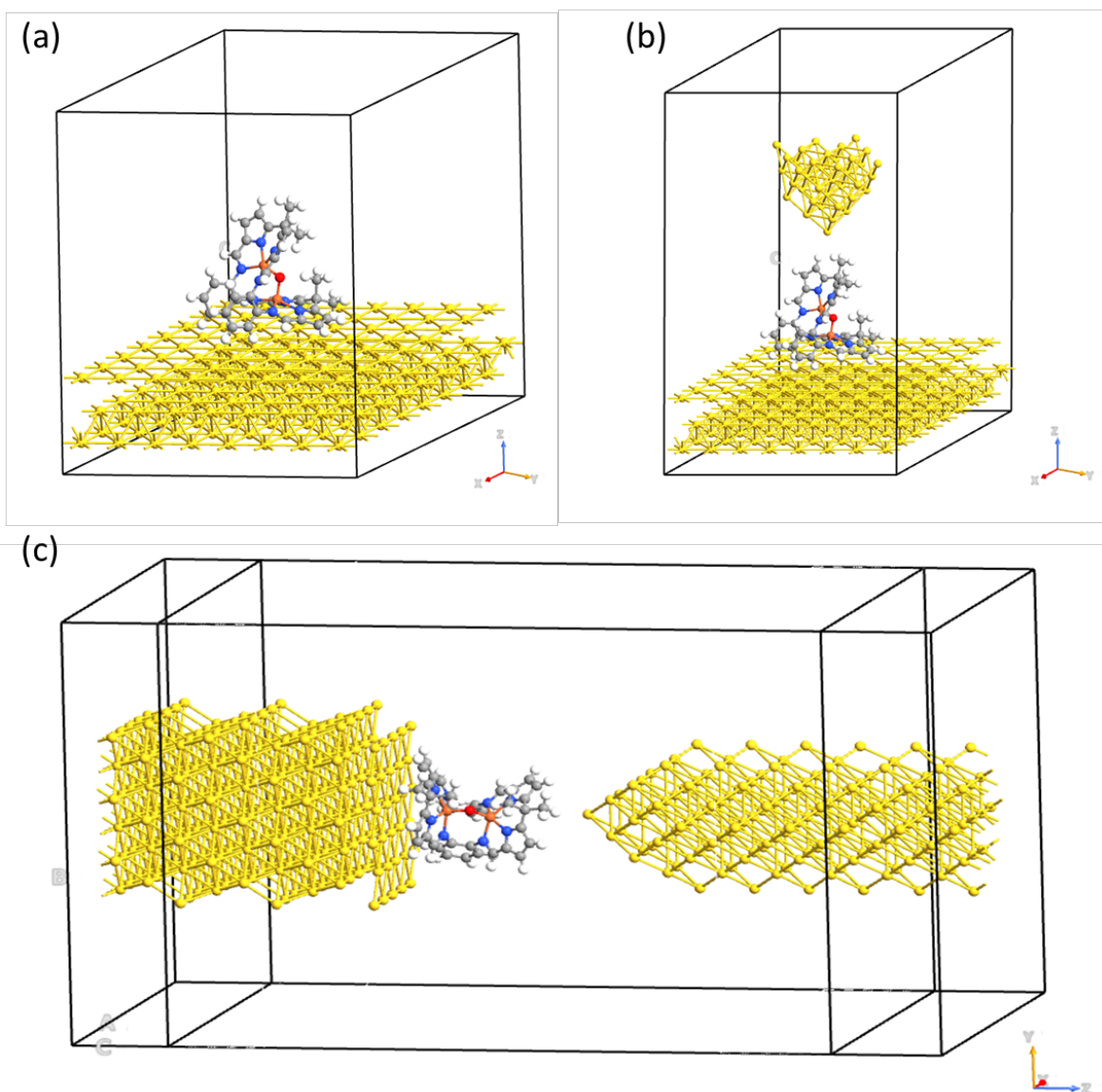


**Figure S3.1.** Depiction of the different unit cells employed in the present work. (a) Slab configuration with 1 deposited over Au(111). (b) Slab configuration with complex 1 deposited over Au(111) interacting with Au pyramidal cluster of 39 atoms. (c) Open system employed in the NEGF-DFT calculations. In this setup, the influence of the Au semi-infinite electrodes over the central zone is included through the electrode's self-energies via the scattering zone Green's function.

### S3.2 Complex 1 frontier orbitals diagrams in the three employed architectures

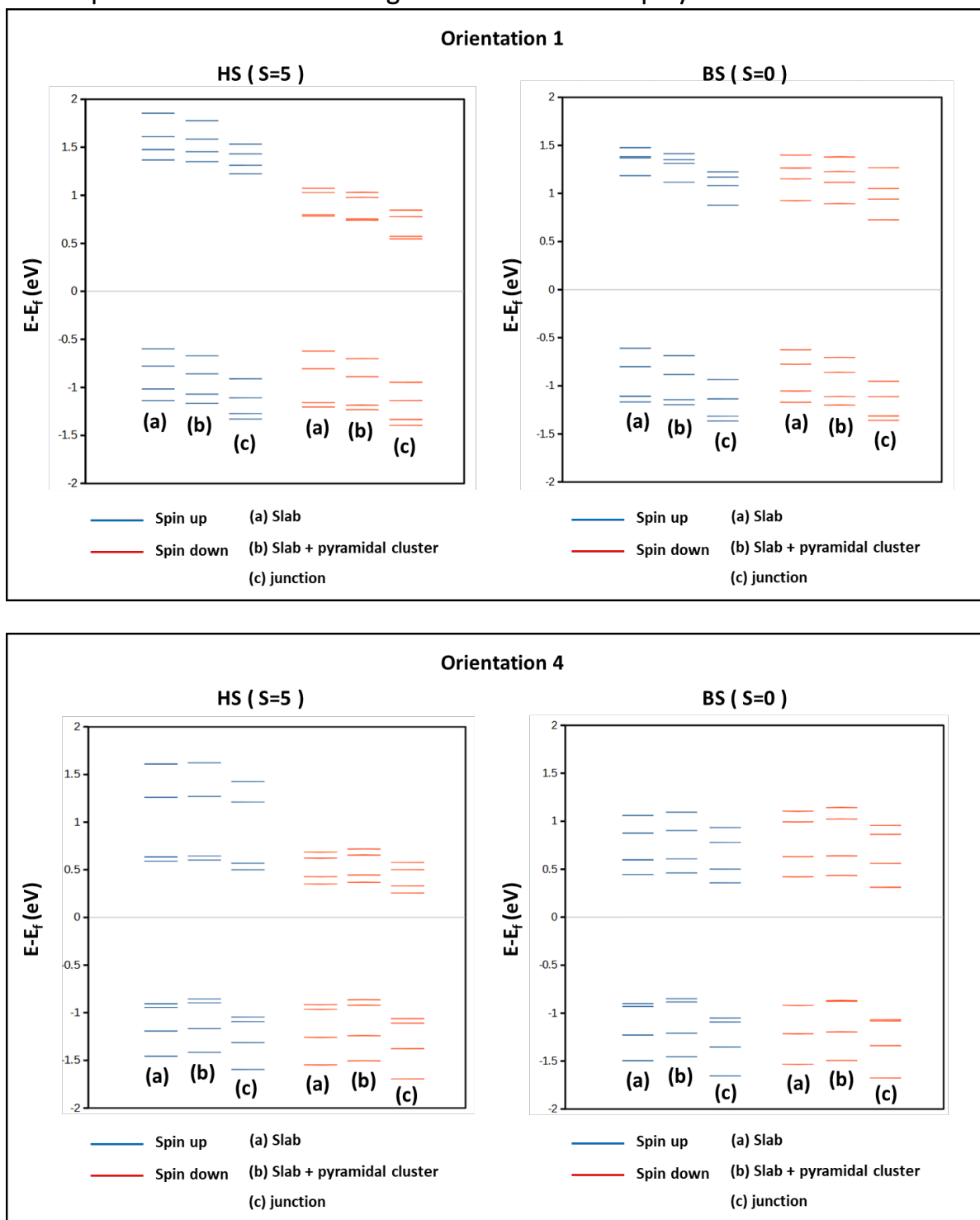


**Figure S3.2** Comparison of the frontier molecular projected self-consistent Hamiltonian (MPSH) states of the complex in the High Spin (HS) and Broken Symmetry (BS) solutions, deposited over the Au(111) surface in (top) orientation 1 and (bottom) orientation 4 employing three different configurations (See Figure S3.1).

### S3.3 Hay, Thibault and Hoffmann (HTH) model

The relationship between the single occupied molecular orbitals of the complex with the coupling constant  $J$  can be studied theoretically using the model introduced by Hay, Thibault and Hoffmann.<sup>28</sup> In this model, the  $J$  value can be directly related to the energy difference between the in-phase ( $\psi_s = \psi_{d_A} + \psi_{d_B}$ ) and out-of-phase ( $\psi_a = \psi_{d_A} - \psi_{d_B}$ ) magnetic orbitals of the complex, where  $\psi_{d_A}$ ,  $\psi_{d_B}$  are d-type orbitals localized on two metallic centers A and B respectively. In the case of just two electrons on two orbitals, centered on sites A and B, respectively, the  $J$  value can be expressed as:

$$E_S - E_T = J = 2K_{AB} - \frac{(\varepsilon_s - \varepsilon_a)^2}{J_{AA} - J_{AB}}$$

where  $J_{AA}$ ,  $J_{AB}$  and are the one and two centered Coulomb repulsion integrals of the localized  $\psi_{d_A}$ ,  $\psi_{d_B}$  orbitals, and  $K_{AB}$  is the exchange integral between  $\psi_{d_A}$ ,  $\psi_{d_B}$ . In the general case of  $m$  unpaired electrons on each center they introduced two expressions for the ferromagnetic ( $J_F$ ) and the antiferromagnetic ( $J_{AF}$ ) contributions to  $J$ :

$$J_F = \sum_{i \in A} \sum_{j \in B} K_{ij}$$
$$J_{AF} = -\frac{1}{m^2} \sum_{i=1}^m \frac{(\varepsilon_s^i - \varepsilon_a^i)^2}{J_{A_i A_i} - J_{A_i B_i}}$$

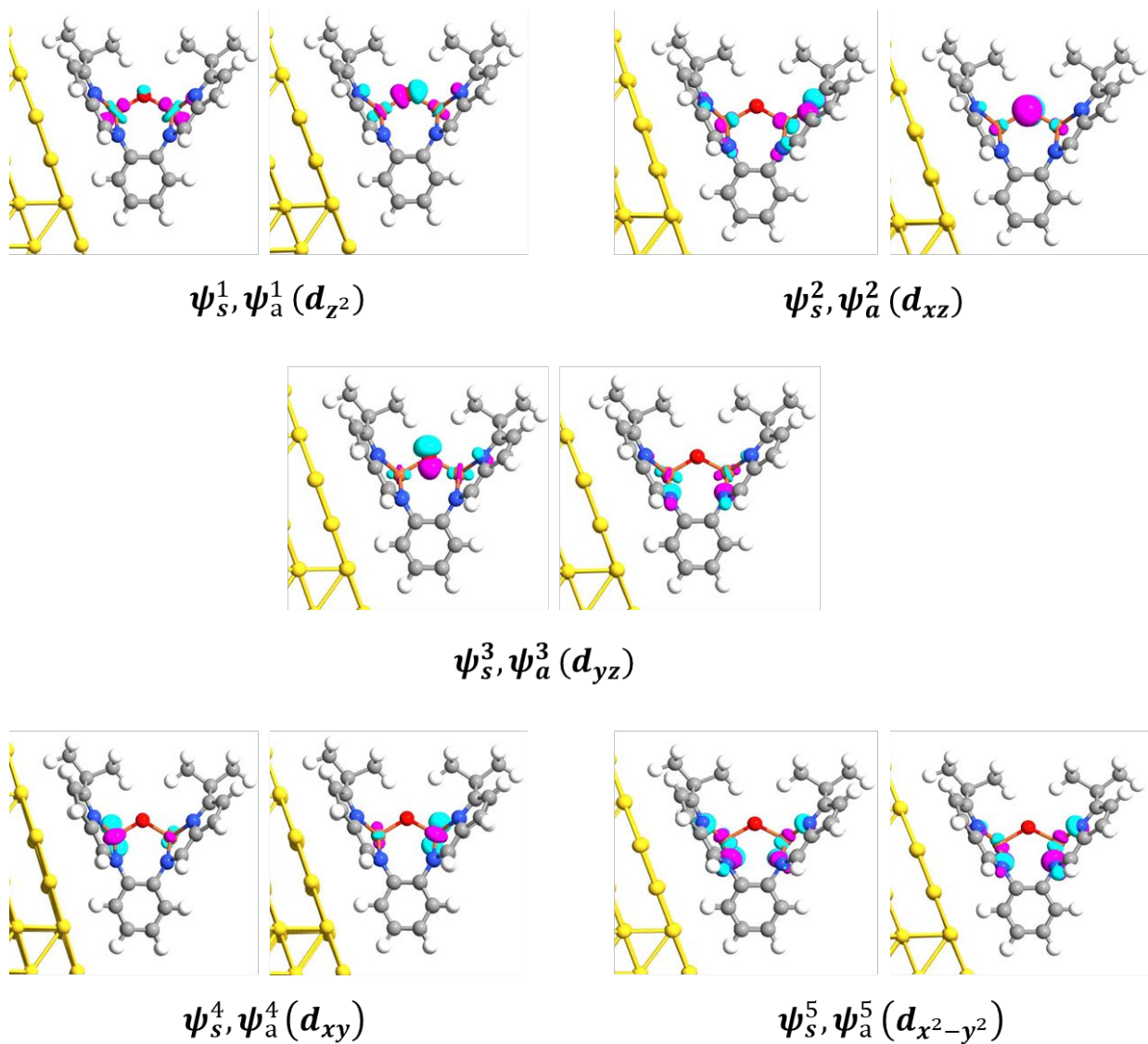


**Figure S3.3.** Molecular projected self-consistent Hamiltonian (MPSH) states on the Fe ions, oxygen bridge and nitrogen atoms of complex 1, in the molecular junction with the latter deposited in orientation 1, employed in the Hay, Thibault and Hoffmann (HTH) analysis. These states correspond to the single occupied magnetic orbitals obtained through CASSCF calculations.

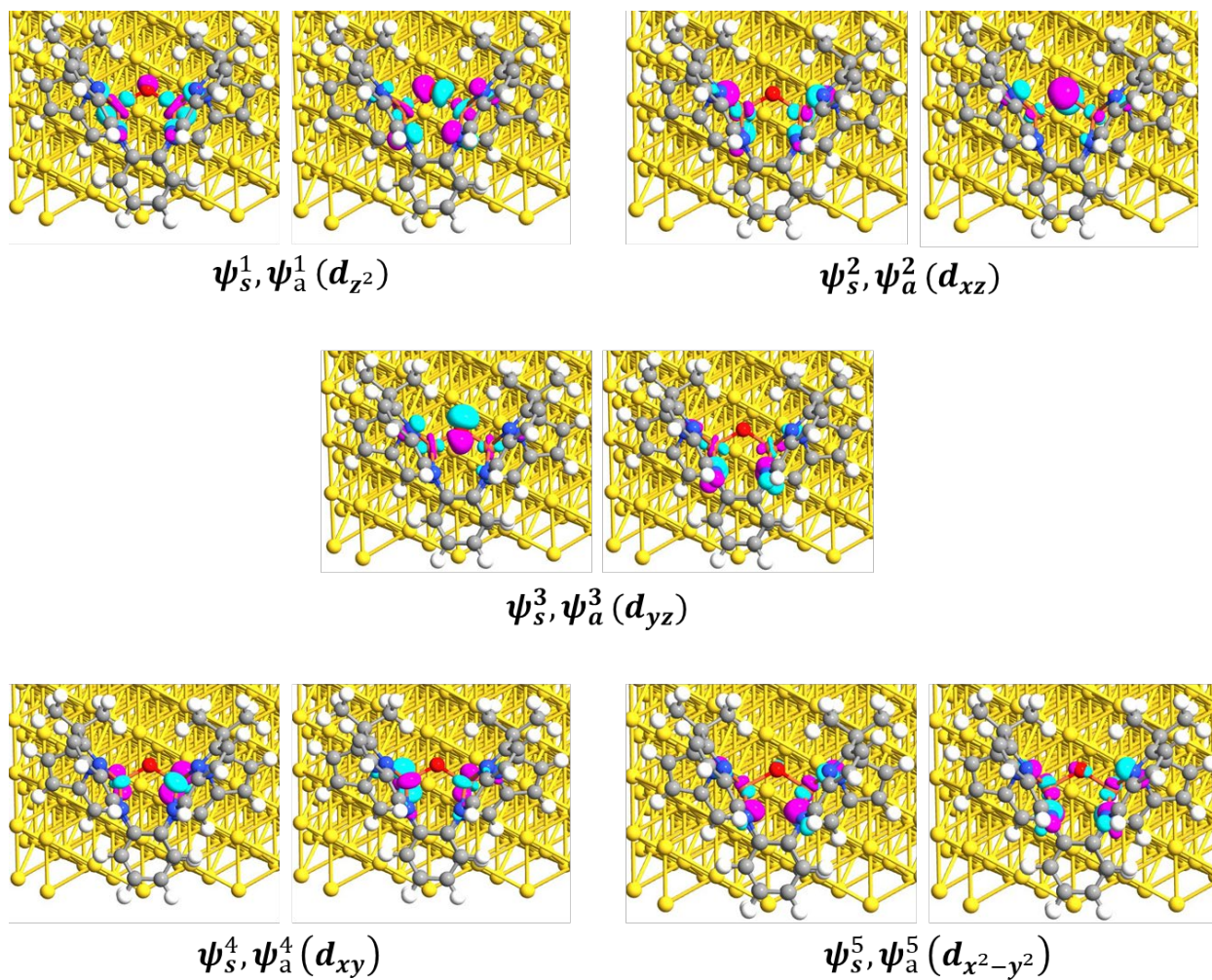


**Figure S3.4** Molecular projected self-consistent Hamiltonian (MPSH) states on the Fe ions, oxygen bridge and nitrogen atoms of complex 1, in the molecular junction with the latter deposited in orientation 4, employed in the Hay, Thibault and Hoffmann (HTH) analysis. These states correspond to the single occupied magnetic orbitals obtained through CASSCF calculations.

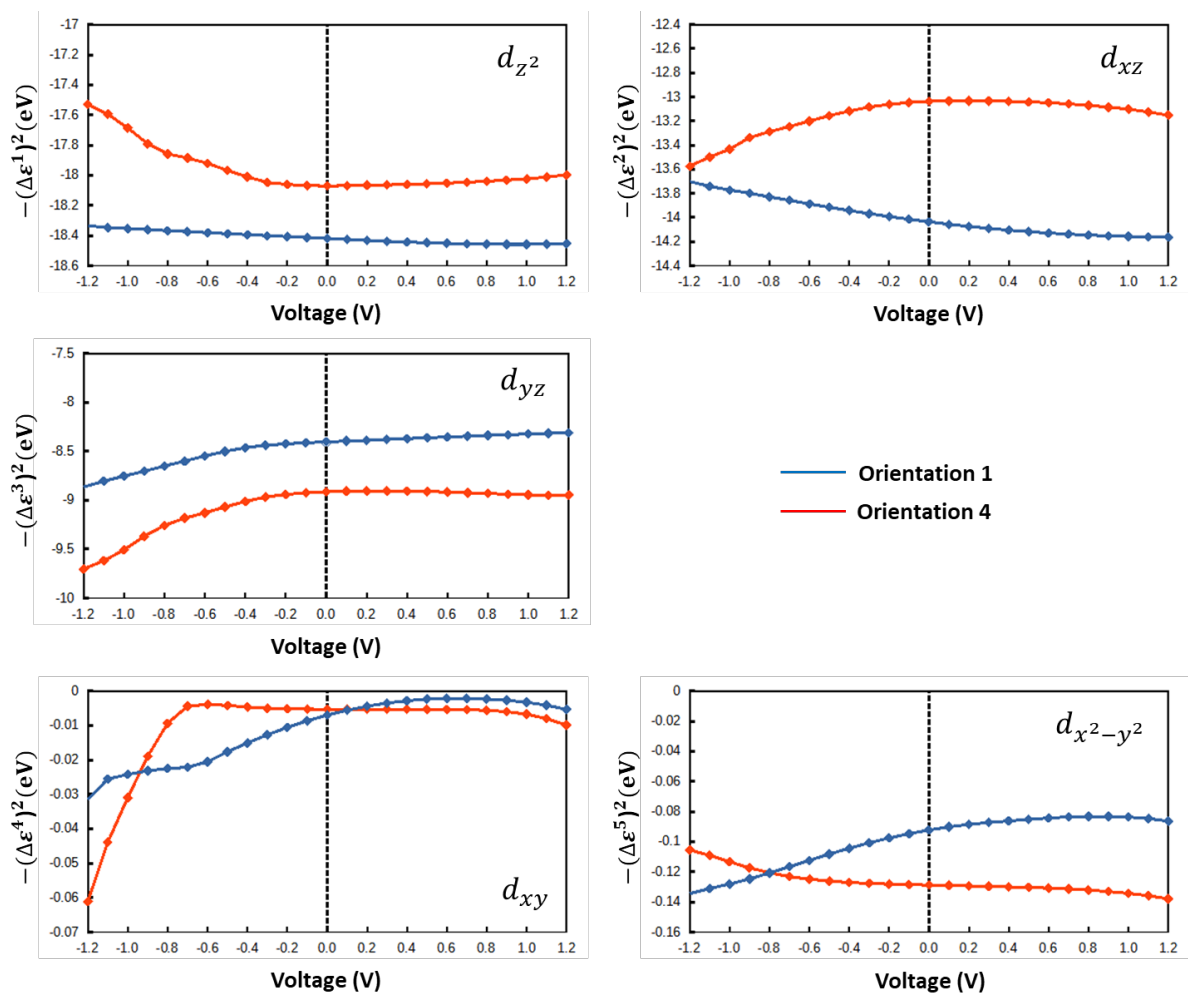


**Figure S3.5.** Voltage dependence of the energy difference between the symmetric ( $\psi_s$ ) and antisymmetric ( $\psi_a$ ) d-type molecular orbitals employed in the Hay, Thibault and Hoffmann (HTH) analysis.

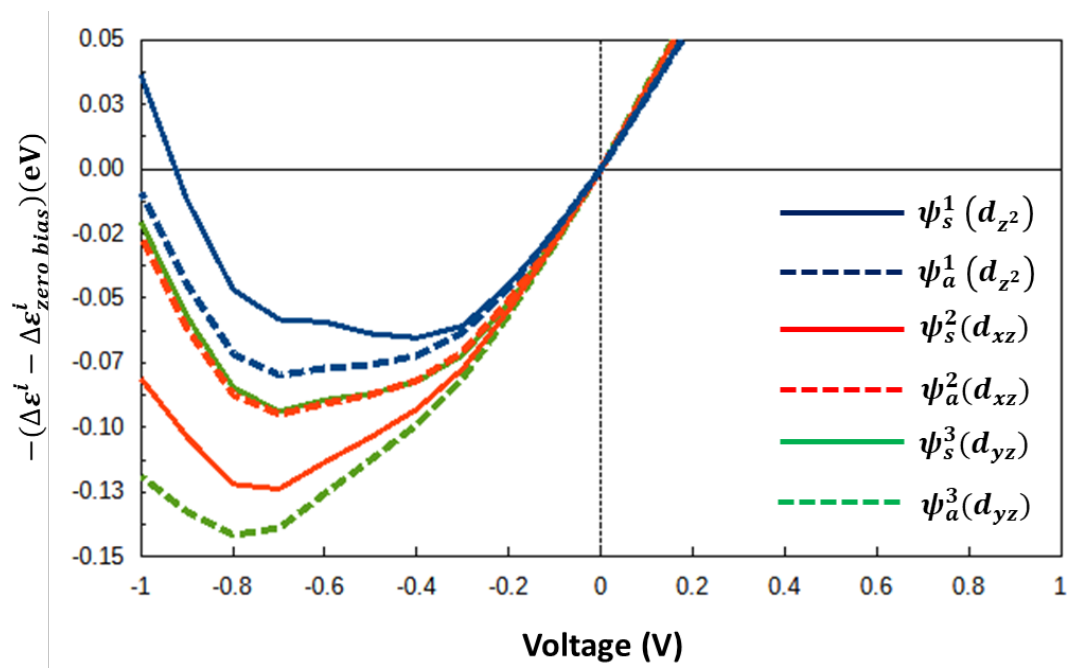


**Figure S3.6.** Voltage dependence stabilization and destabilization (with respect to their corresponding energies at zero bias) of the  $d_{z^2}$ ,  $d_{xz}$  and  $d_{yz}$  molecular orbitals employed in the Hay, Thibault and Hoffmann (HTH) analysis.

### S3.4 Effects of a homogeneous electric field in the complex in gas phase

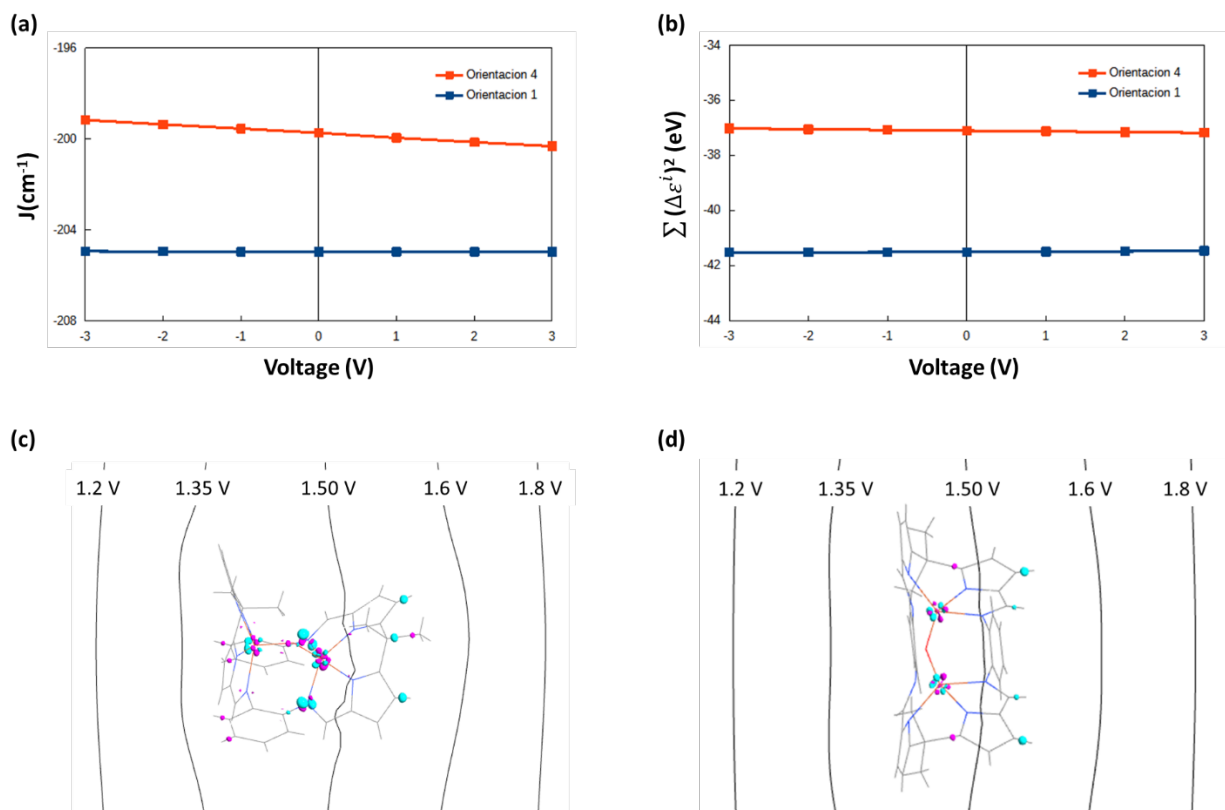


**Figure S3.7.** (a) Coupling constant  $J$  computed through the BS methodology in complex 1 in gas phase, employing the molecular geometry adopted by it on each deposition orientation, under the effects of a homogeneous electric field, simulated by placing the complex between two large metallic square plates separated by 90 Å, at a potential difference of 1,2, and 3 V. (b) Voltage dependence of the sum of the energy differences between the corresponding symmetric ( $\psi_s$ ) and antisymmetric ( $\psi_a$ ) d-type molecular orbitals employed in the Hay, Thibault and Hoffmann (HTH) analysis. (c, d) Induced charge densities and electrostatic potential isolines applying a bias voltage of 3V. In the plots, magenta/cyan represent excess/deficiency of charge with respect to respective system at zero bias. All the iso surfaces were set to 3.5E-4 1/bohr<sup>3</sup>.

### S3.5 Potential iso-isolines and voltage-induced charge density in the junction setup

#### S3.5.1 Orientation 4

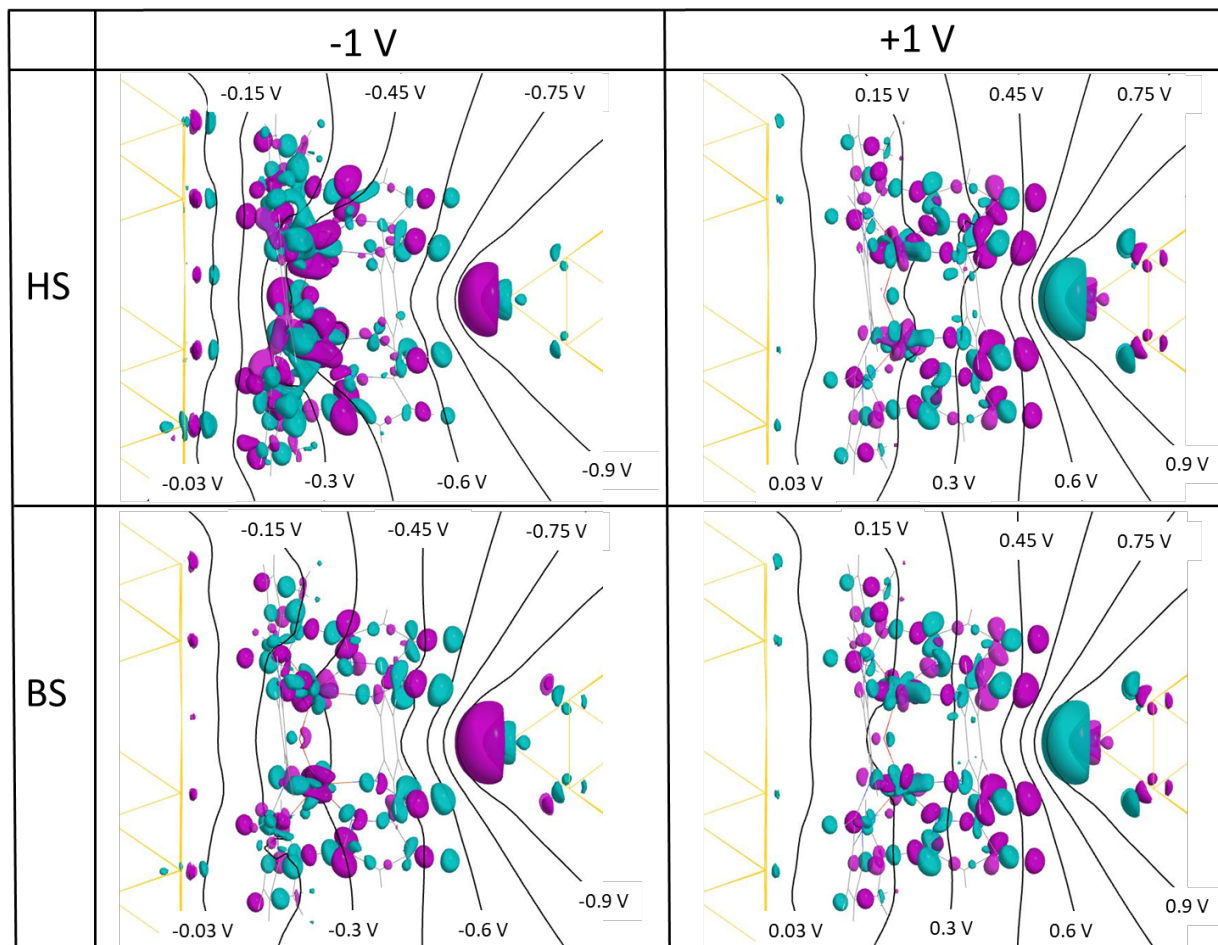


**Figure S3.8** Induced charge densities and electrostatic potential isolines in the junctions featuring complex 1 deposited over the Au(111) surface in orientation 4, in both HS and BS states, and applying a bias voltage of -1V and +1V. In the plots, magenta/cyan represent excess/deficiency of charge with respect to respective system at zero bias. All the iso surfaces were set to  $3.5E-4$  1/bohr<sup>3</sup>.

### S3.5.2 Orientation 1

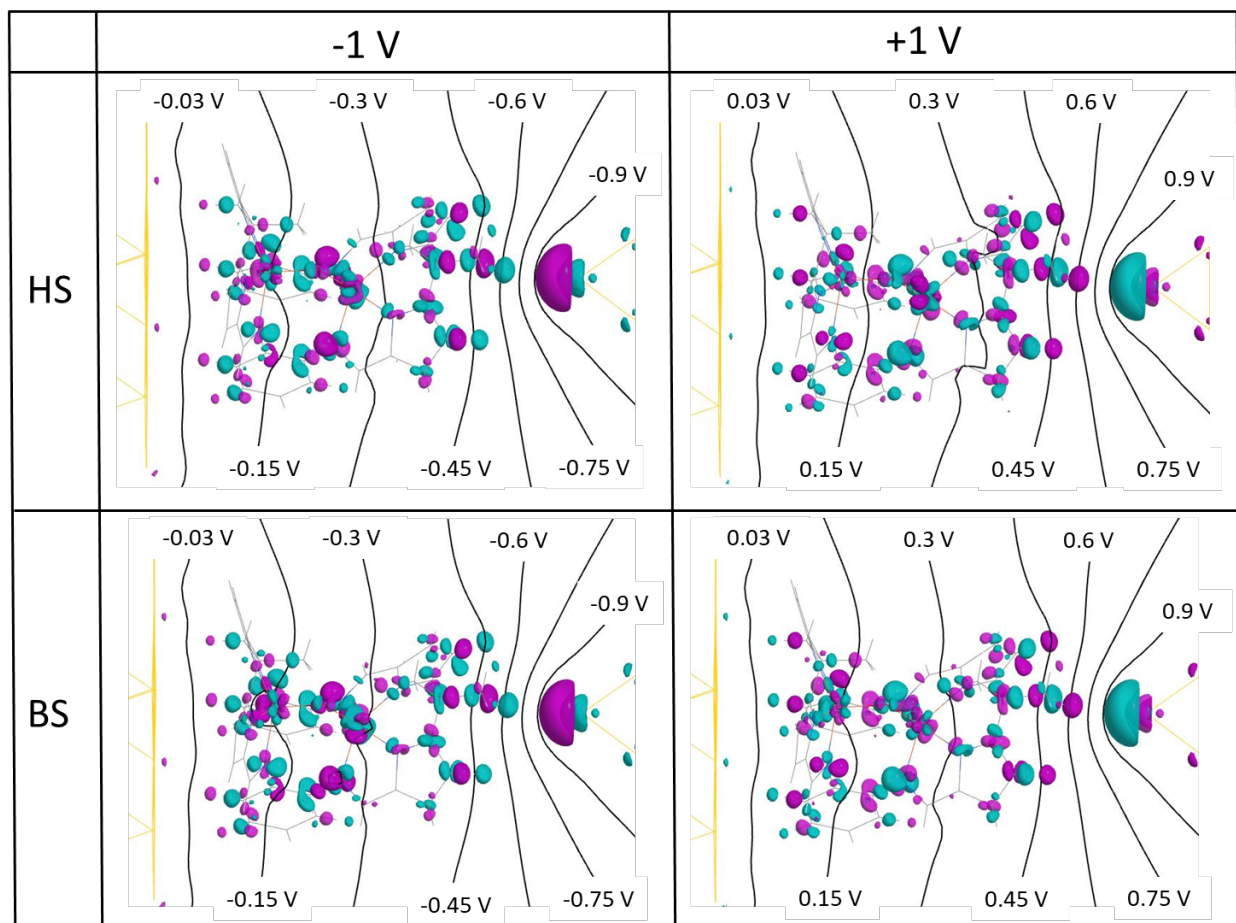
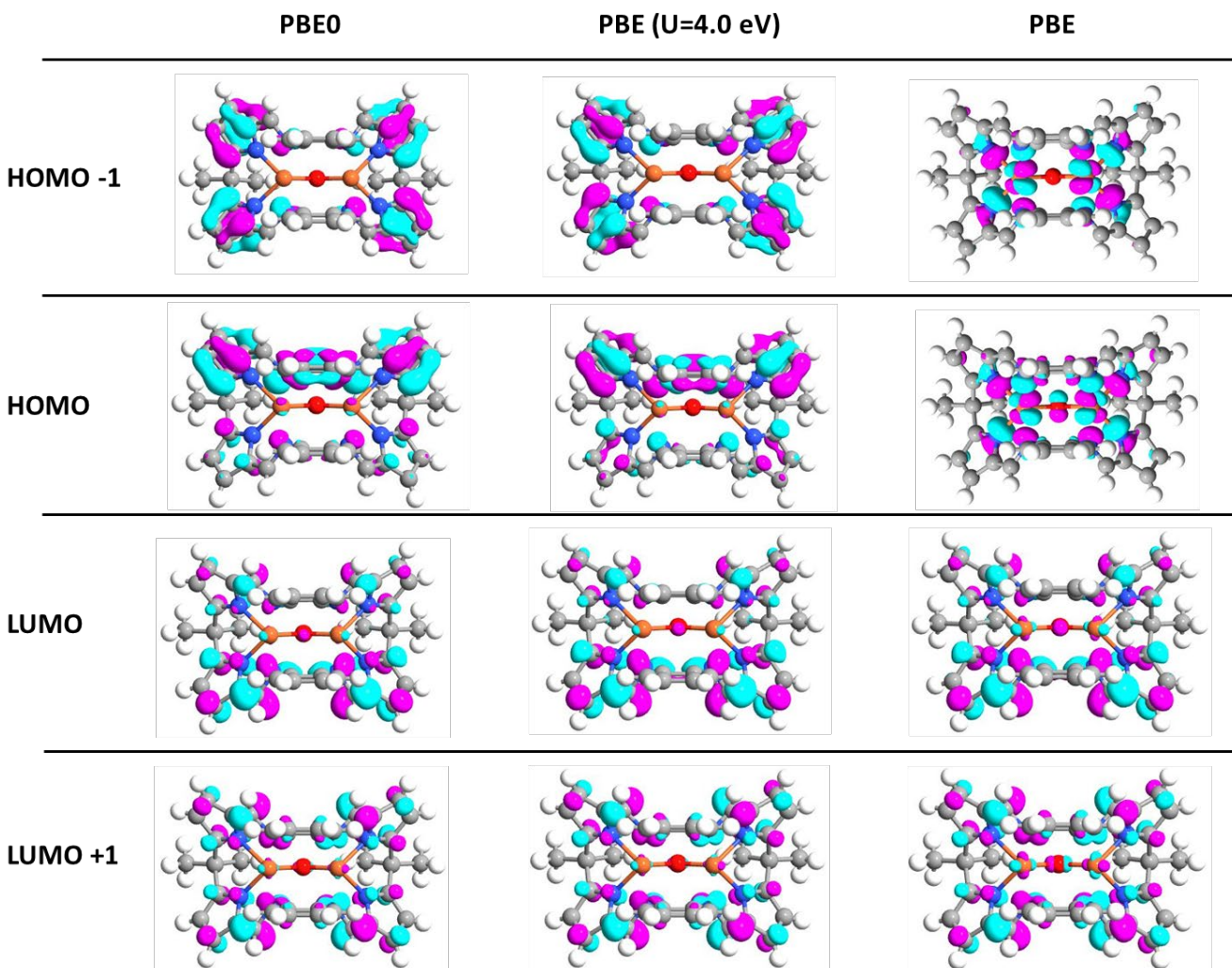


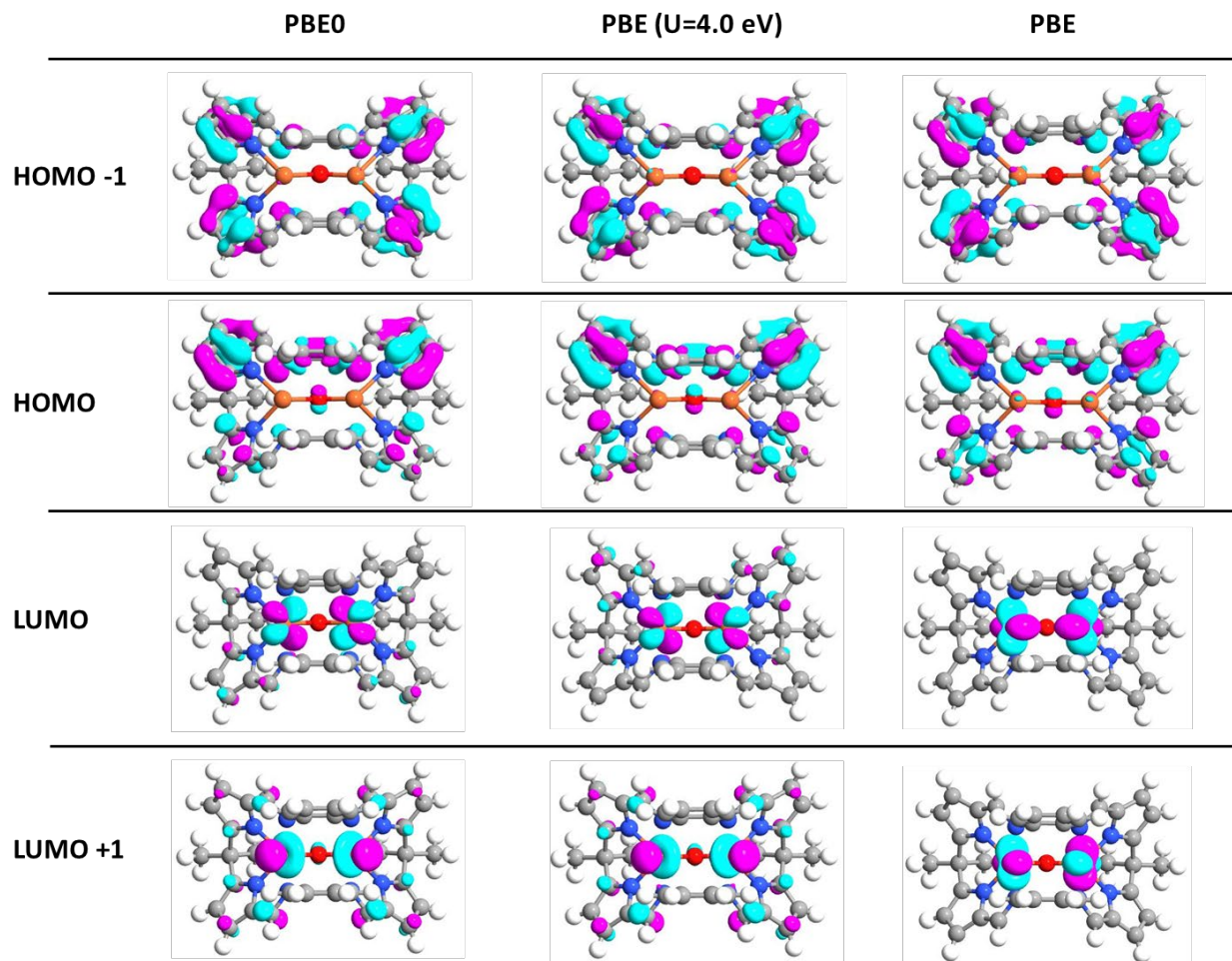
**Figure S3.9** Induced charge densities and electrostatic potential isolines in the junctions featuring complex 1 deposited over the Au(111) surface in orientation 1, in both HS and BS states, and applying a bias voltage of -1V and +1V. In the plots, magenta/cyan represent excess/deficiency of charge with respect to respective system at zero bias. All the iso surfaces were set to  $3.5E-4$   $1/\text{bohr}^3$ .

## S4. Frontier orbitals of the isolated complex

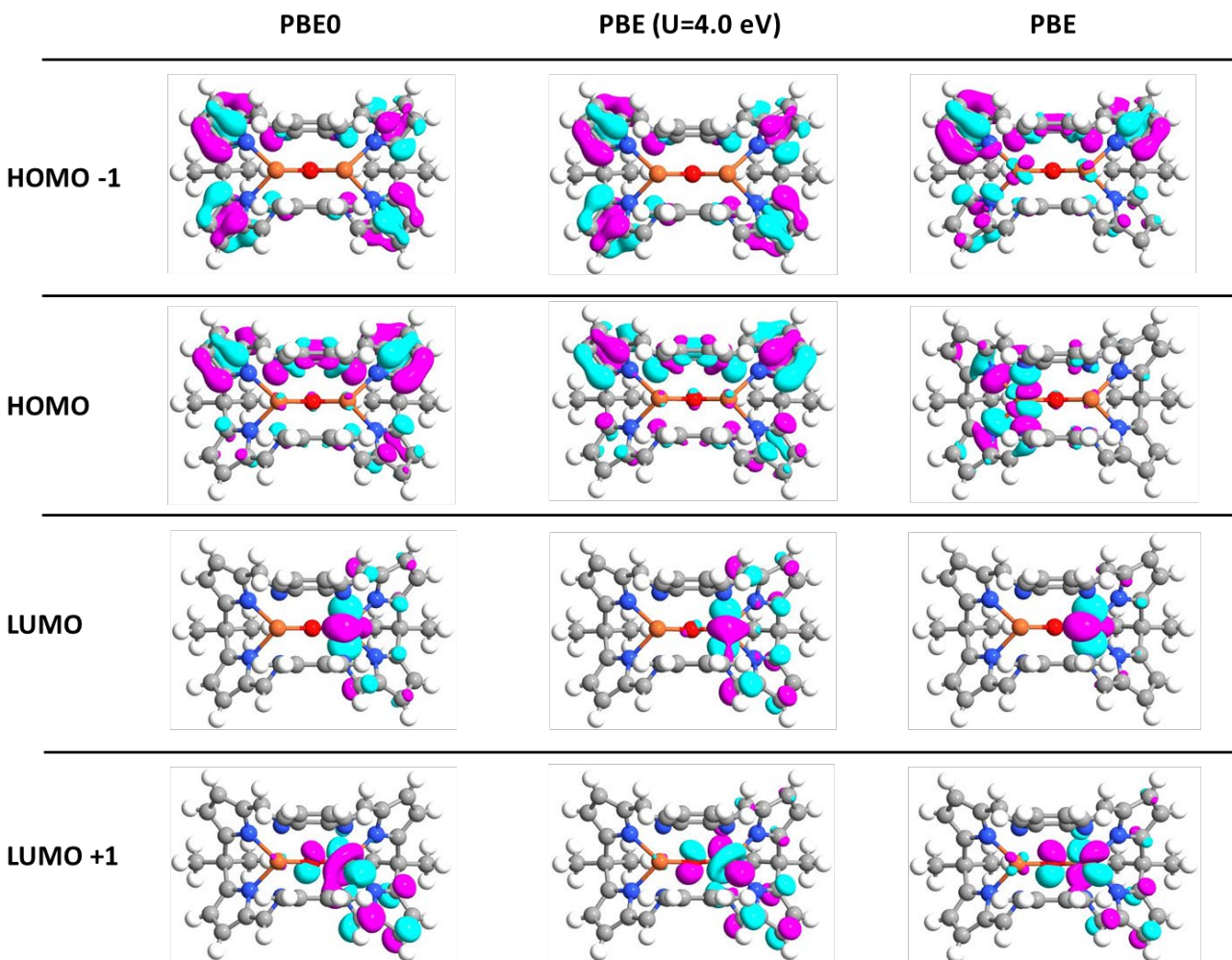
### S4.1. High Spin (HS) spin up frontier orbitals



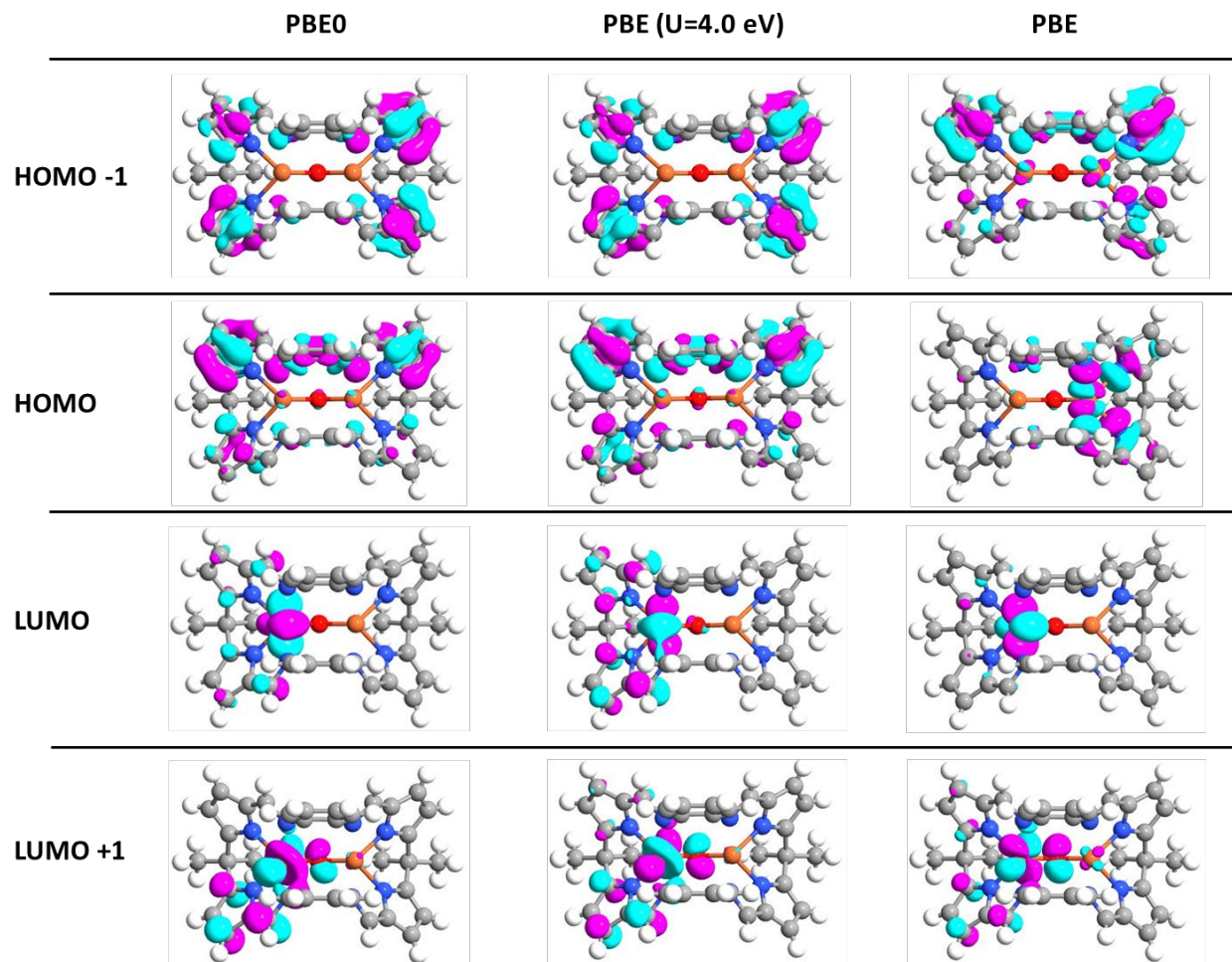
## S4.2. High Spin (HS) spin down frontier orbitals



### S4.3. Broken Symmetry (BS) spin up frontier orbitals



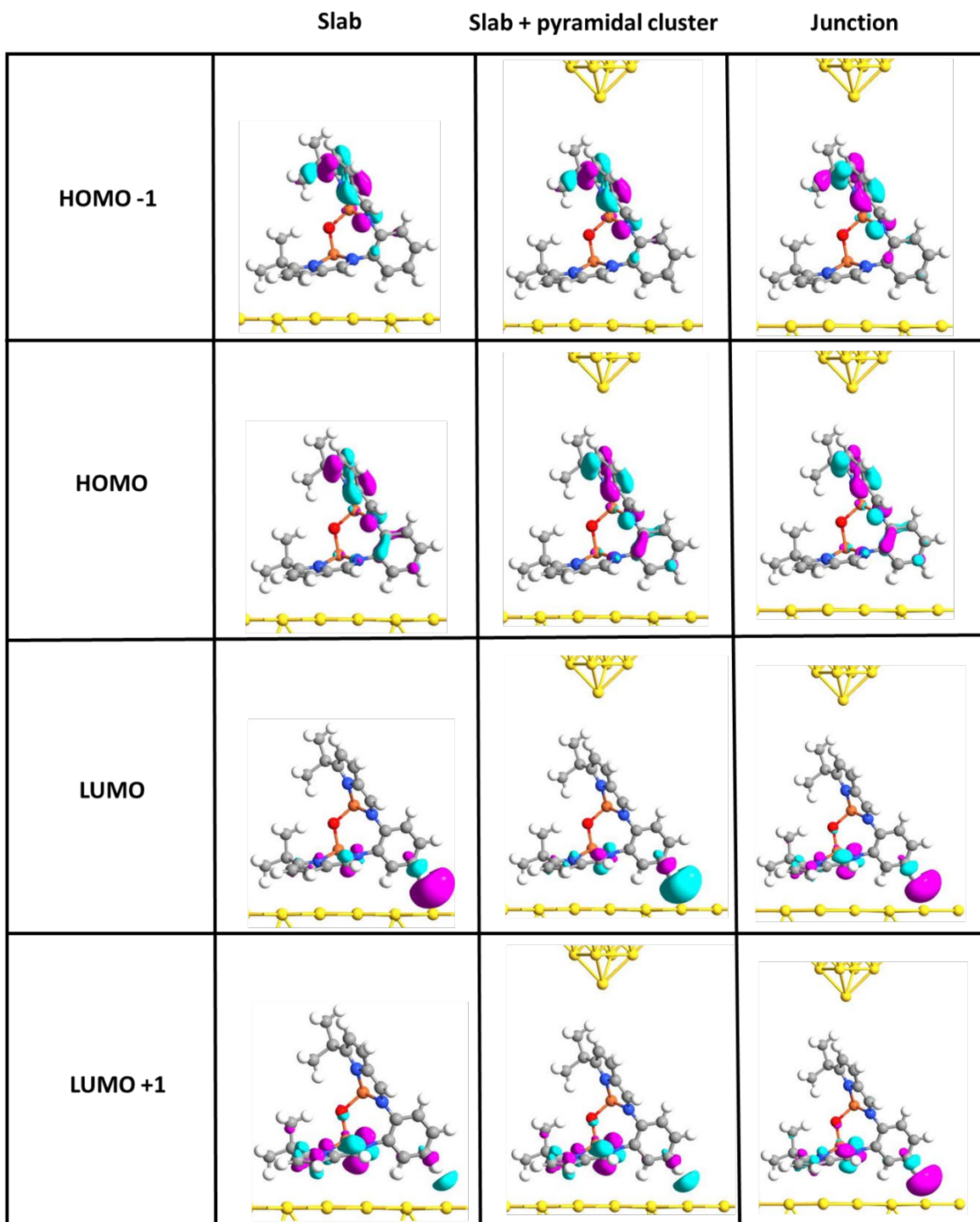
### S4.3. Broken Symmetry (BS) spin down frontier orbitals



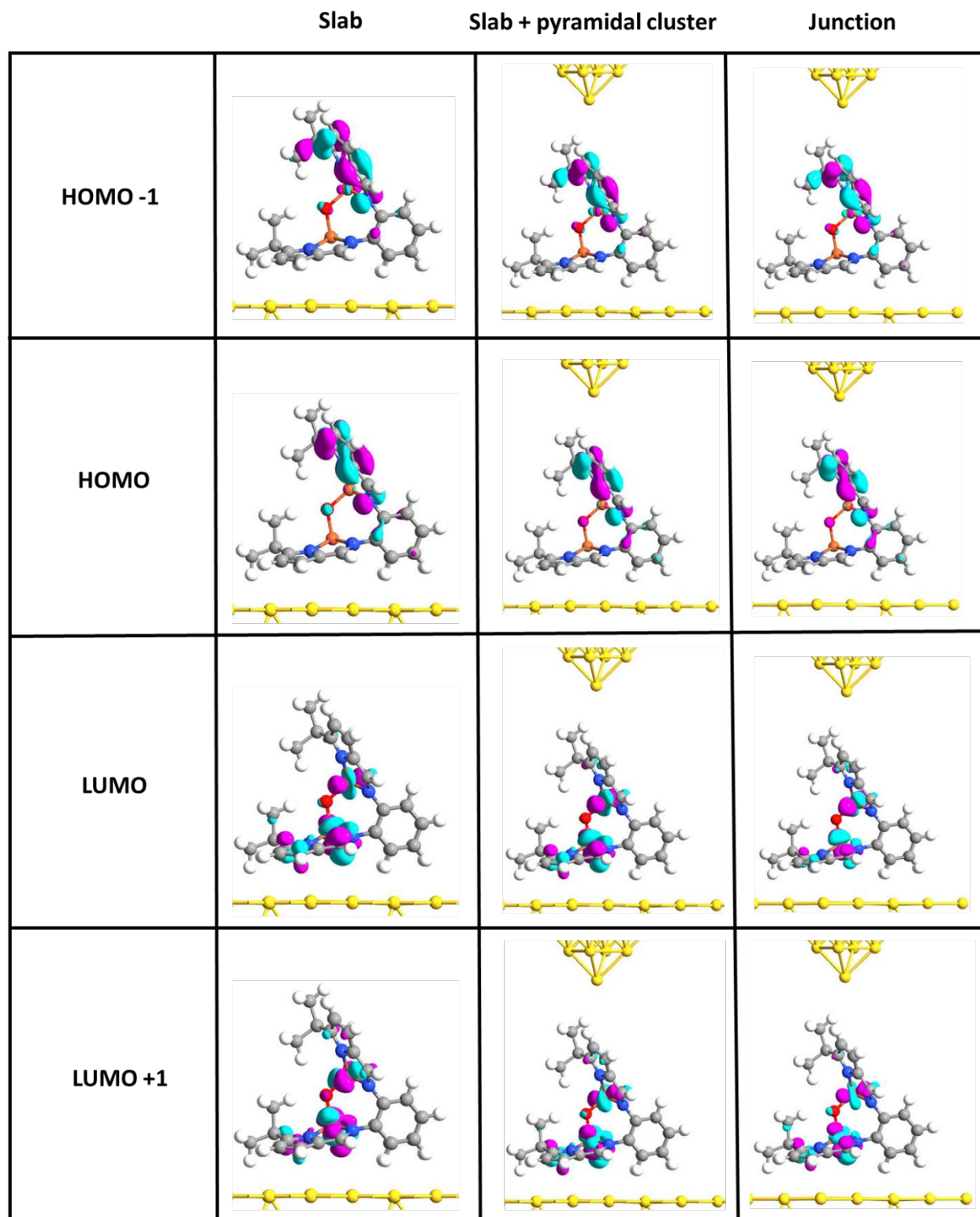
## S5. Molecular projected self-consistent Hamiltonian (MPSH) states of the complex

### S5.1. Orientation 1

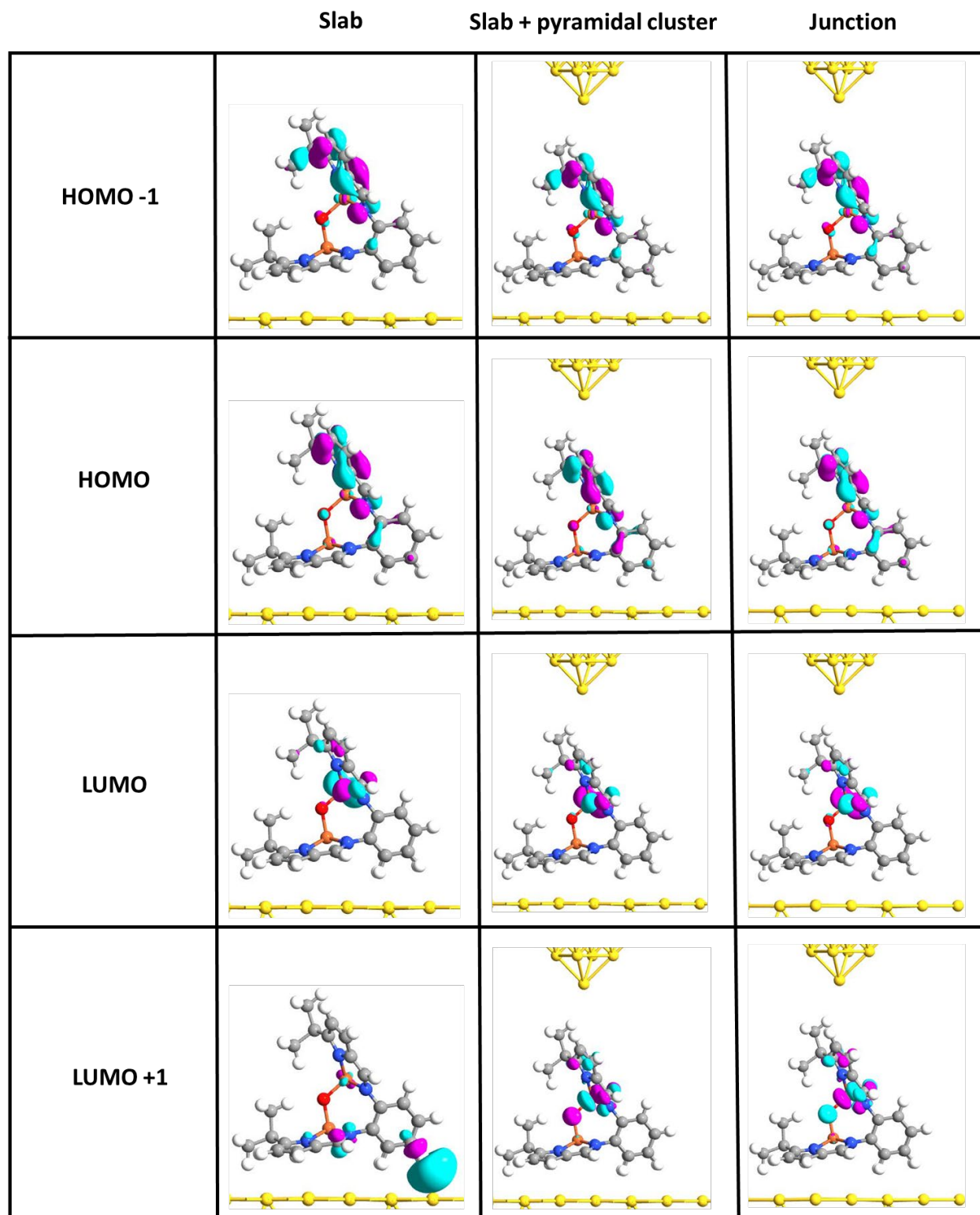
#### S5.1.1 High Spin (HS) spin up frontier orbitals



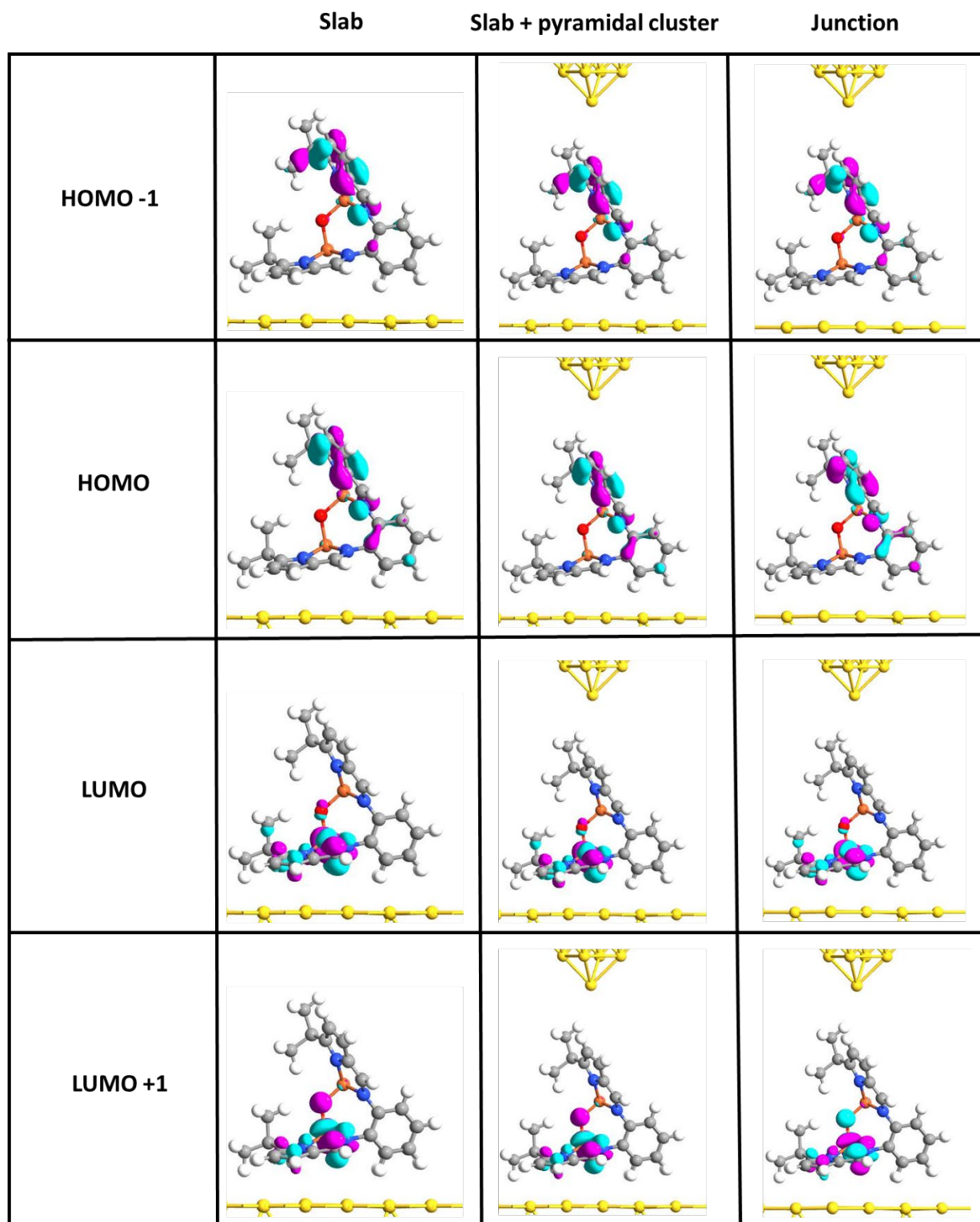
### S5.1.2 High Spin (HS) spin down frontier orbitals



### S5.1.3 Broken Symmetry (BS) spin up frontier orbitals

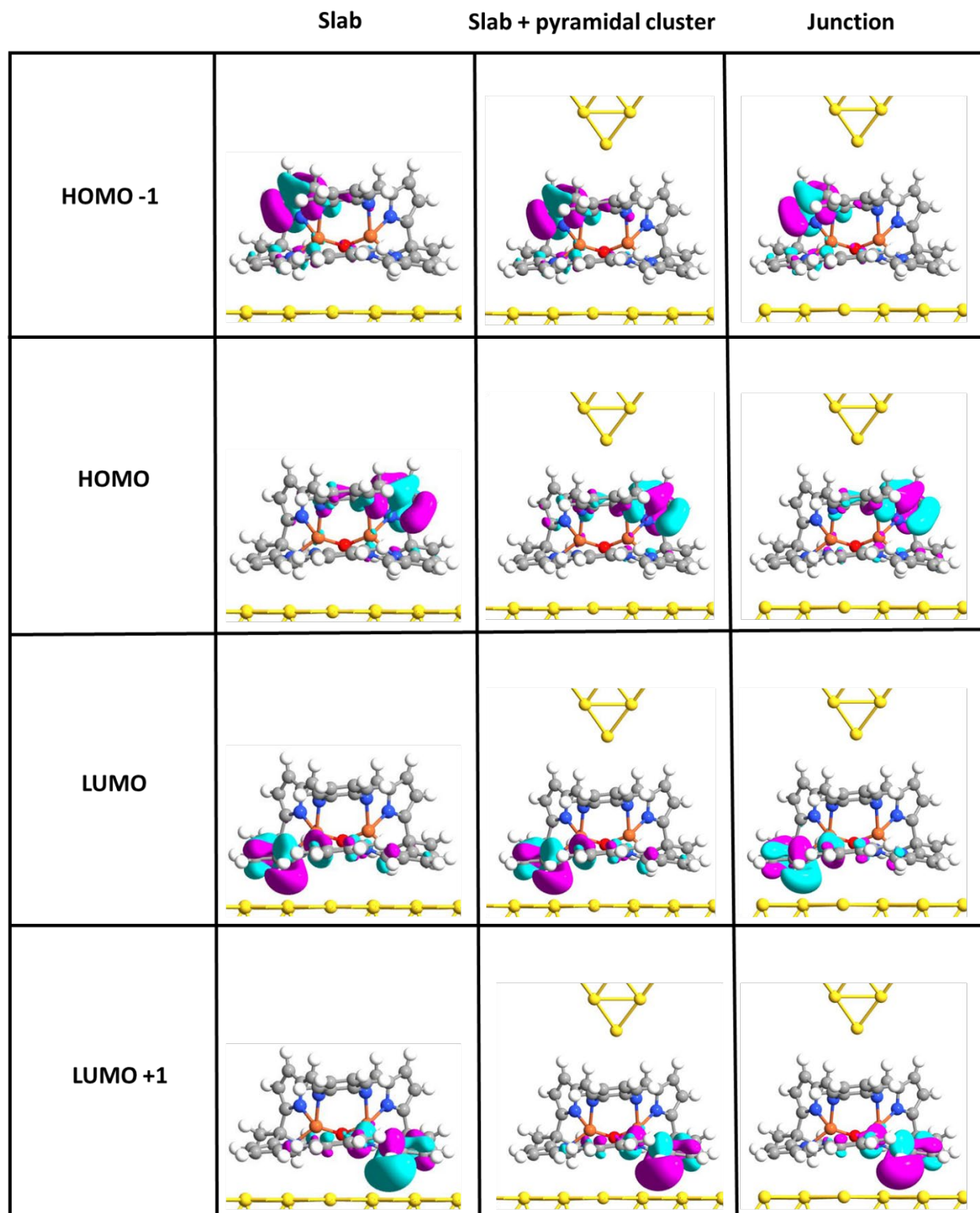


### S5.1.4 Broken Symmetry (BS) spin down frontier orbitals

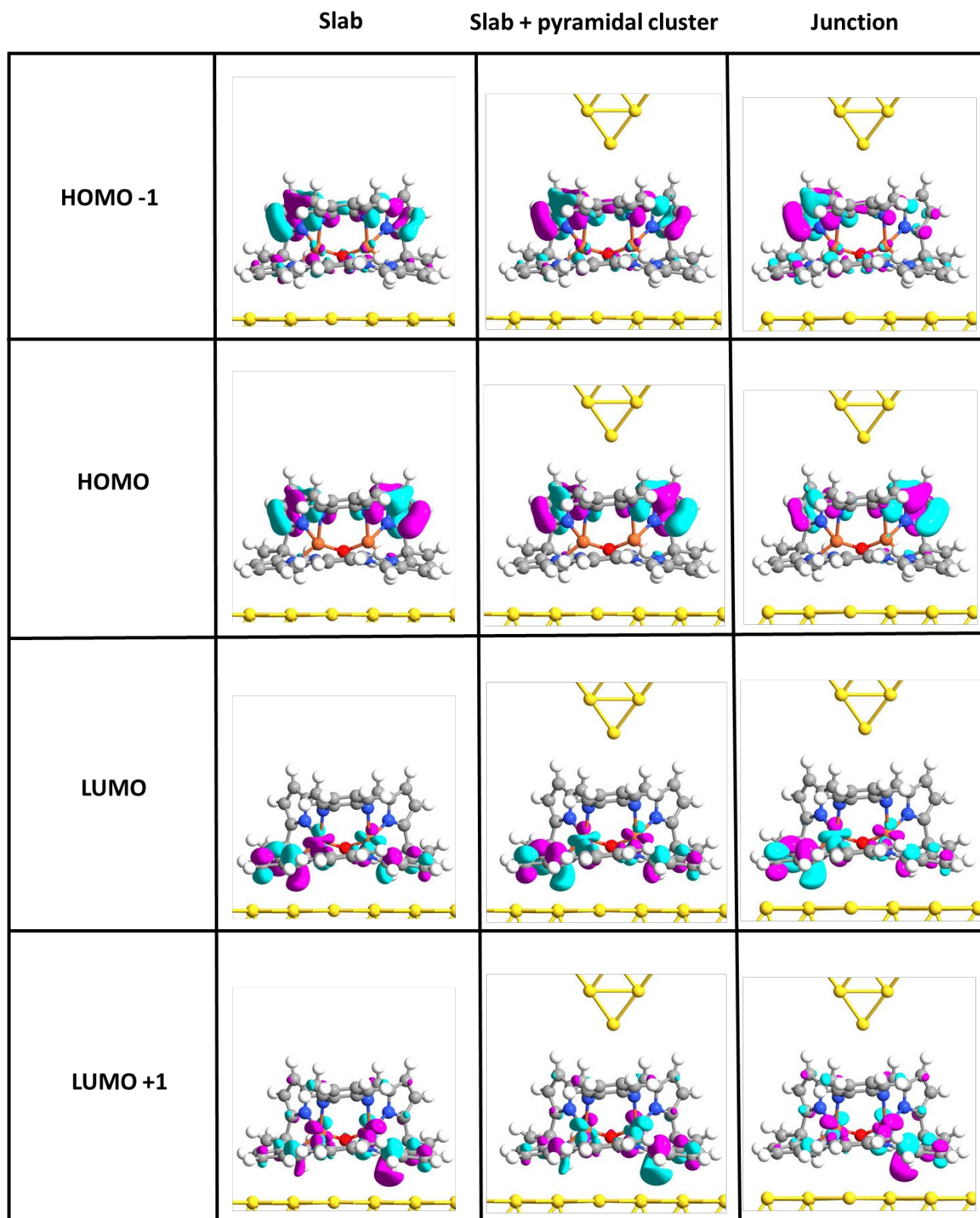


## S5.2. Orientation 4

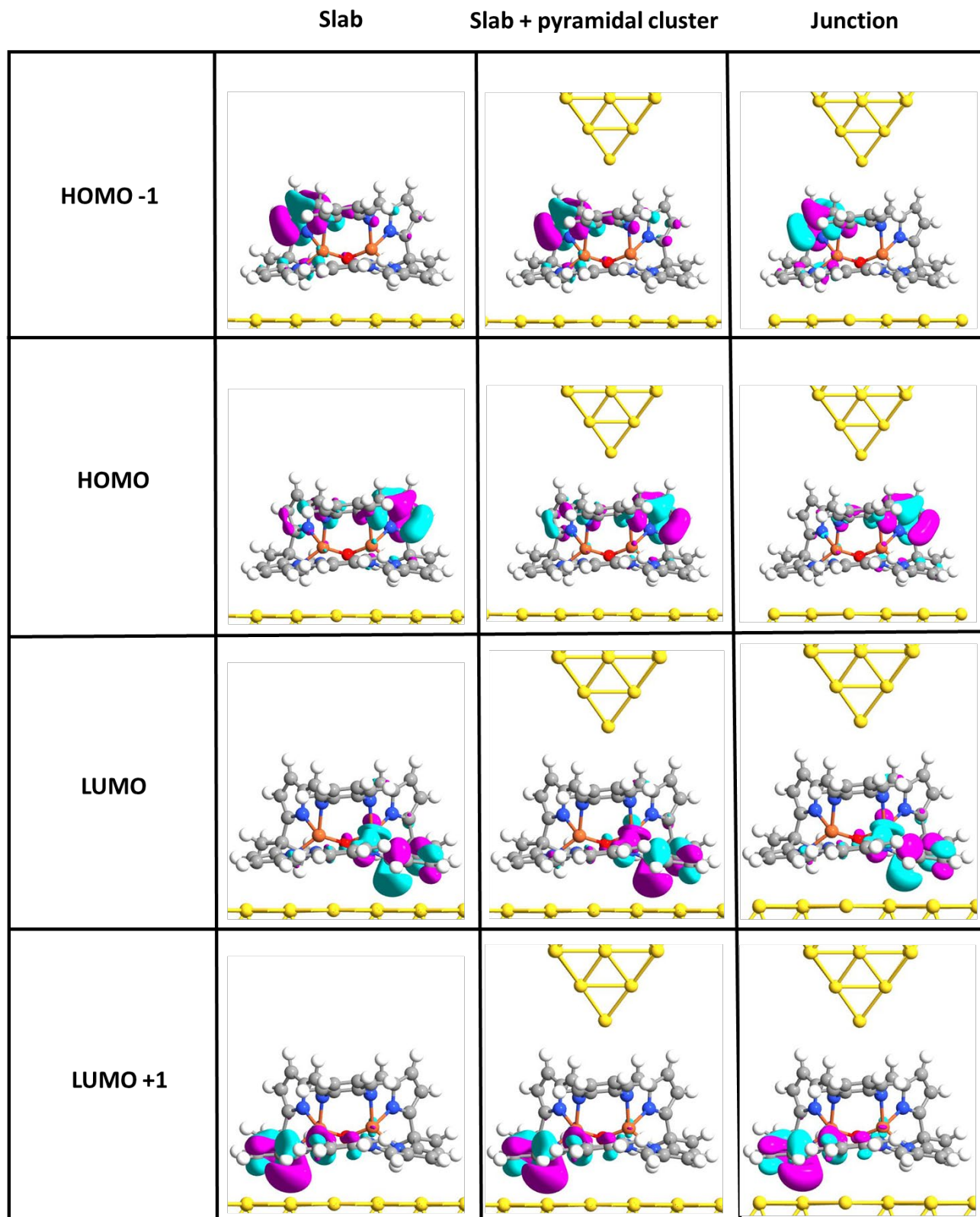
### S5.2.1 High Spin (HS) spin up frontier orbitals



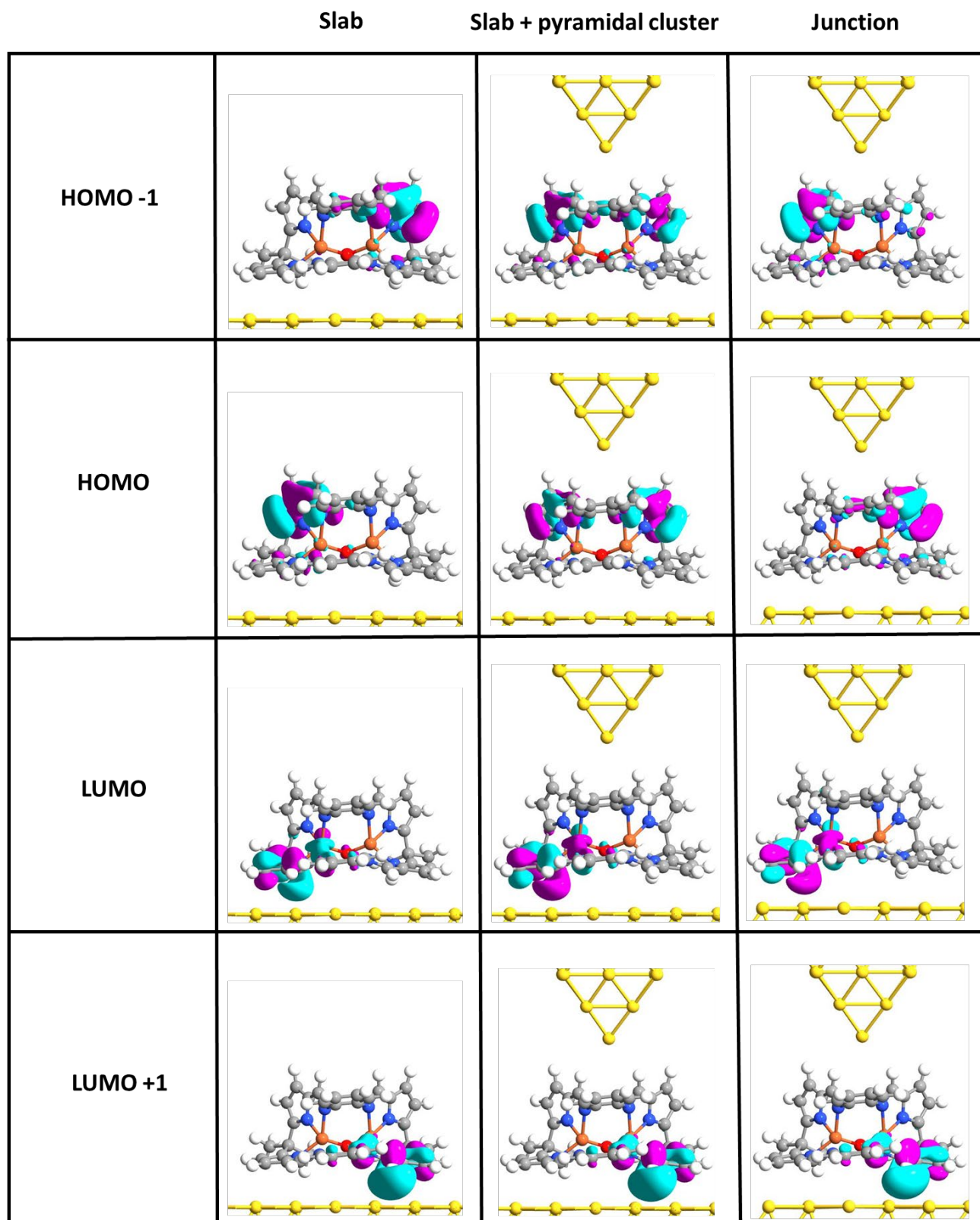
### S5.2.2 High Spin (HS) spin down frontier orbitals



### S5.2.3 Broken Symmetry (BS) spin up frontier orbitals



### S5.2.4 Broken Symmetry (BS) spin down frontier orbitals



## References

- (1) Gatteschi, D.; Sessoli, R.; Villain, J. *Molecular nanomagnets*; Oxford University Press, 2006.
- (2) Noodleman, L. Valence bond description of antiferromagnetic coupling in transition metal dimers. *The Journal of Chemical Physics* **1981**, *74* (10), 5737-5743. DOI: 10.1063/1.440939 (accessed 2018/12/17).
- (3) Soda, T.; Kitagawa, Y.; Onishi, T.; Takano, Y.; Shigeta, Y.; Nagao, H.; Yoshioka, Y.; Yamaguchi, K. Ab initio computations of effective exchange integrals for H–H, H–He–H and Mn2O2 complex: comparison of broken-symmetry approaches. *Chemical Physics Letters* **2000**, *319* (3), 223-230. DOI: [https://doi.org/10.1016/S0009-2614\(00\)00166-4](https://doi.org/10.1016/S0009-2614(00)00166-4).
- (4) Valero, R.; Costa, R.; de P. R. Moreira, I.; Truhlar, D. G.; Illas, F. Performance of the M06 family of exchange-correlation functionals for predicting magnetic coupling in organic and inorganic molecules. *The Journal of Chemical Physics* **2008**, *128* (11), 114103. DOI: 10.1063/1.2838987 (accessed 2018/12/17).
- (5) Ruiz, E.; Alvarez, S.; Cano, J.; Polo, V. About the calculation of exchange coupling constants using density-functional theory: The role of the self-interaction error. *The Journal of Chemical Physics* **2005**, *123* (16). DOI: 10.1063/1.2085171 (accessed 1/31/2024).
- (6) Rivero, P.; Moreira Ide, P.; Illas, F.; Scuseria, G. E. Reliability of range-separated hybrid functionals for describing magnetic coupling in molecular systems. *J Chem Phys* **2008**, *129* (18), 184110. DOI: 10.1063/1.3006419 From NIm.
- (7) Adamo, C.; Barone, V. Toward reliable density functional methods without adjustable parameters: The PBE0 model. *The Journal of Chemical Physics* **1999**, *110* (13), 6158-6170. DOI: 10.1063/1.478522 (accessed 1/30/2024).
- (8) Kotaru, S.; Kähler, S.; Alessio, M.; Krylov, A. I. Magnetic exchange interactions in binuclear and tetranuclear iron(III) complexes described by spin-flip DFT and Heisenberg effective Hamiltonians. *Journal of Computational Chemistry* **2023**, *44* (3), 367-380. DOI: <https://doi.org/10.1002/jcc.26941>.
- (9) Mukherjee, R. N.; Stack, T. D. P.; Holm, R. H. Angle dependence of the properties of the [Fe2X]4+ bridge unit (X = O, S): structures, antiferromagnetic coupling, and properties in solution. *Journal of the American Chemical Society* **1988**, *110* (6), 1850-1861. DOI: 10.1021/ja00214a030.
- (10) Mabbs, F. E.; McLachlan, V. N.; McFadden, D.; McPhail, A. T. Magnetic properties and crystal and molecular structure of  $\mu$ -oxo-bis[bis-(2-methyl-8-hydroxyquinolino)iron(III)]-chloroform. *Journal of the Chemical Society, Dalton Transactions* **1973**, (19), 2016-2021, 10.1039/DT9730002016. DOI: 10.1039/DT9730002016.
- (11) Coggon, P.; McPhail, A. T.; Mabbs, F. E.; McLachlan, V. N. Crystal and molecular structure and magnetic anisotropy of  $\mu$ -oxo-bis-[NN'-ethylenebis(salicylideneiminato)iron(III)]-dichloromethane. *Journal of the Chemical Society A: Inorganic, Physical, Theoretical* **1971**, (0), 1014-1019, 10.1039/J19710001014. DOI: 10.1039/J19710001014.
- (12) Landrum, J. T.; Grimmett, D.; Haller, K. J.; Scheidt, W. R.; Reed, C. A. Imidazolate- and oxo-bridged metalloporphyrins. *Journal of the American Chemical Society* **1981**, *103* (10), 2640-2650. DOI: 10.1021/ja00400a027.
- (13) Perdew, J. P.; Burke, K.; Ernzerhof, M. Generalized Gradient Approximation Made Simple [Phys. Rev. Lett. *77*, 3865 (1996)]. *Physical Review Letters* **1997**, *78* (7), 1396-1396. DOI: 10.1103/PhysRevLett.78.1396.
- (14) Anisimov, V. I.; Zaanen, J.; Andersen, O. K. Band theory and Mott insulators: Hubbard U instead of Stoner I. *Physical Review B* **1991**, *44* (3), 943-954. DOI: 10.1103/PhysRevB.44.943.
- (15) Liechtenstein, A. I.; Anisimov, V. I.; Zaanen, J. Density-functional theory and strong interactions: Orbital ordering in Mott-Hubbard insulators. *Physical Review B* **1995**, *52* (8), R5467-R5470. DOI: 10.1103/PhysRevB.52.R5467.

- (16) Anisimov, V. I.; Poteryaev, A. I.; Korotin, M. A.; Anokhin, A. O.; Kotliar, G. First-principles calculations of the electronic structure and spectra of strongly correlated systems: dynamical mean-field theory. *Journal of Physics: Condensed Matter* **1997**, *9* (35), 7359. DOI: 10.1088/0953-8984/9/35/010.
- (17) Meng, X.; Möller, J.; Mansouri, M.; Sánchez-Portal, D.; Garcia-Lekue, A.; Weismann, A.; Li, C.; Herges, R.; Berndt, R. Controlling the Spin States of FeTBrPP on Au(111). *ACS Nano* **2022**. DOI: 10.1021/acsnano.2c09310.
- (18) Liu, B.; Fu, H.; Guan, J.; Shao, B.; Meng, S.; Guo, J.; Wang, W. An Iron-Porphyrin Complex with Large Easy-Axis Magnetic Anisotropy on Metal Substrate. *ACS Nano* **2017**, *11* (11), 11402-11408. DOI: 10.1021/acsnano.7b06029.
- (19) Gueddida, S.; Gruber, M.; Miyamachi, T.; Beaurepaire, E.; Wulfhekkel, W.; Alouani, M. Exchange Coupling of Spin-Crossover Molecules to Ferromagnetic Co Islands. *The Journal of Physical Chemistry Letters* **2016**, *7* (5), 900-904. DOI: 10.1021/acs.jpcclett.6b00172.
- (20) Karuppannan, S. K.; Martín-Rodríguez, A.; Ruiz, E.; Harding, P.; Harding, D. J.; Yu, X.; Tadich, A.; Cowie, B.; Qi, D.; Nijhuis, C. A. Room temperature conductance switching in a molecular iron(III) spin crossover junction. *Chemical Science* **2021**, *12* (7), 2381-2388, 10.1039/D0SC04555A. DOI: 10.1039/D0SC04555A.
- (21) Zhao, P.; Gao, X.-J.; Song, Y.; Li, X.-X.; Chen, G. Spin-filtering, giant magnetoresistance, negative differential resistance effects and spin logic gate in P2TA-O2-based molecular junction with different transition metal atoms. *Organic Electronics* **2018**, *57*, 104-109. DOI: <https://doi.org/10.1016/j.orgel.2018.03.007>.
- (22) Gallego-Planas, N.; Martín-Rodríguez, A.; Ruiz, E. Magnetic and transport properties of Fe<sub>4</sub> single-molecule magnets: a theoretical insight. *Dalton Transactions* **2016**, *45* (47), 18867-18875, 10.1039/C6DT03460H. DOI: 10.1039/C6DT03460H.
- (23) Martín-Rodríguez, A.; Aravena, D.; Ruiz, E. DFT approaches to transport calculations in magnetic single-molecule devices. *Theoretical Chemistry Accounts* **2016**, *135* (8), 192. DOI: 10.1007/s00214-016-1941-6.
- (24) Smidstrup, S.; Markussen, T.; Vancaeyveld, P.; Wellendorff, J.; Schneider, J.; Gunst, T.; Verstichel, B.; Stradi, D.; Khomyakov, P. A.; Vej-Hansen, U. G.; et al. QuantumATK: an integrated platform of electronic and atomic-scale modelling tools. *Journal of Physics: Condensed Matter* **2019**, *32* (1), 015901. DOI: 10.1088/1361-648x/ab4007.
- (25) van Setten, M. J.; Giantomassi, M.; Bousquet, E.; Verstraete, M. J.; Hamann, D. R.; Gonze, X.; Rignanese, G. M. The PseudoDojo: Training and grading a 85 element optimized norm-conserving pseudopotential table. *Computer Physics Communications* **2018**, *226*, 39-54. DOI: <https://doi.org/10.1016/j.cpc.2018.01.012>.
- (26) Grimme, S.; Antony, J.; Ehrlich, S.; Krieg, H. A consistent and accurate ab initio parametrization of density functional dispersion correction (DFT-D) for the 94 elements H-Pu. *The Journal of Chemical Physics* **2010**, *132* (15), 154104. DOI: 10.1063/1.3382344.
- (27) Taylor, J.; Guo, H.; Wang, J. Ab initio modeling of quantum transport properties of molecular electronic devices. *Physical Review B* **2001**, *63* (24), 245407. DOI: 10.1103/PhysRevB.63.245407.
- (28) Hay, P. J.; Thibault, J. C.; Hoffmann, R. Orbital interactions in metal dimer complexes. *Journal of the American Chemical Society* **1975**, *97* (17), 4884-4899. DOI: 10.1021/ja00850a018.